Studies on the Preparation of Nanostructured Materials with Sputter-deposition of Metal onto Ionic Liquids and Chemical Reactions in Solution

Toshimasa Suzuki

Referee-in-chief: **Professor Tsukasa Torimoto**
Nagoya University

Referees: **Professor Susumu Kuwabata**
Osaka University

Professor Toshinobu Yogo
Nagoya University

AssociateProfessor Hisao Yoshida
Nagoya University

Contents

Chapter 1 General Introduction

1.1 Introduction

Metal and semiconductor nanoparticles with small diameters and a narrow size distribution have received intense attention in scientific research and industrial application, because they exhibit unique properties depending their size and shape.[1-31] Catalytic activities of metal nanoparticles are strongly affected by their size due to the enlargement of surface-to-volume ratios.[32,33] The metal nanoparticles such as gold (Au) and silver (Ag), exhibit unique optical properties a localized surface plasmon resonance (LSPR) absorption, its wavelength of is greatly varied by controlling the size and shape of nanoparticles.[34-40]

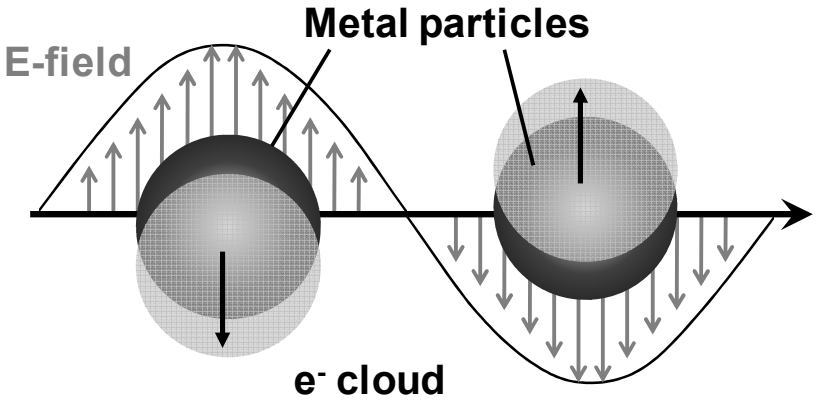

Figre1.1 Schematic illustration of plasmon oscillation for a metal nanoparticle

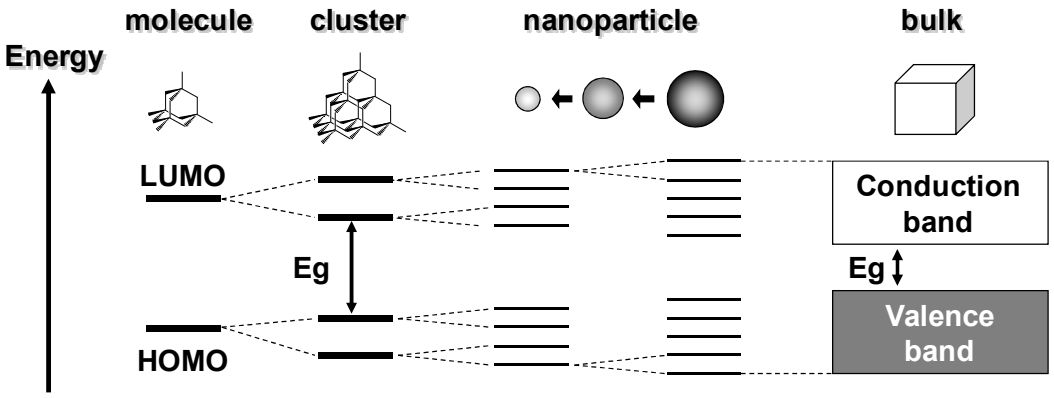

Figure 1.2 Schematic illustrations of energy diagrams for semiconductor nanoparticles in the size between molecules and bulk semiconductors.

The photoexcitation of LSPR produce a locally enhance electric field in the proximity of metal nanoparticles (Figure 1.1), which is utilized for several applications, such as fluorescence enhancement for the detection of biomolecules,[41-43] analysis with surface enhanced Raman scattering,[44,45] and plasmon induced photochemical reactions.[46,47] On the other hand, semiconductor nanoparticles exhibit the remarkable quantum size effects when charge carriers (electrons and holes) are confined in a small nanoparticle with the diameter less than twice the Bohr radius of excitation in the bulk material (Figure 1.2). [48-56] The quantum size effects begin to be appeared less than about 10 nm in its size, being dependent on the kind of semiconductor materials. Decreasing the size of semiconductor nanoparticles, their energy gap generally increase. Hence the energy levels of the conduction band (CB) and valence band (VB) of nanoparticles vary depending on the size of nanoparticles; the smaller size has, higher and lower energy levels of CB and VB, respectively. These

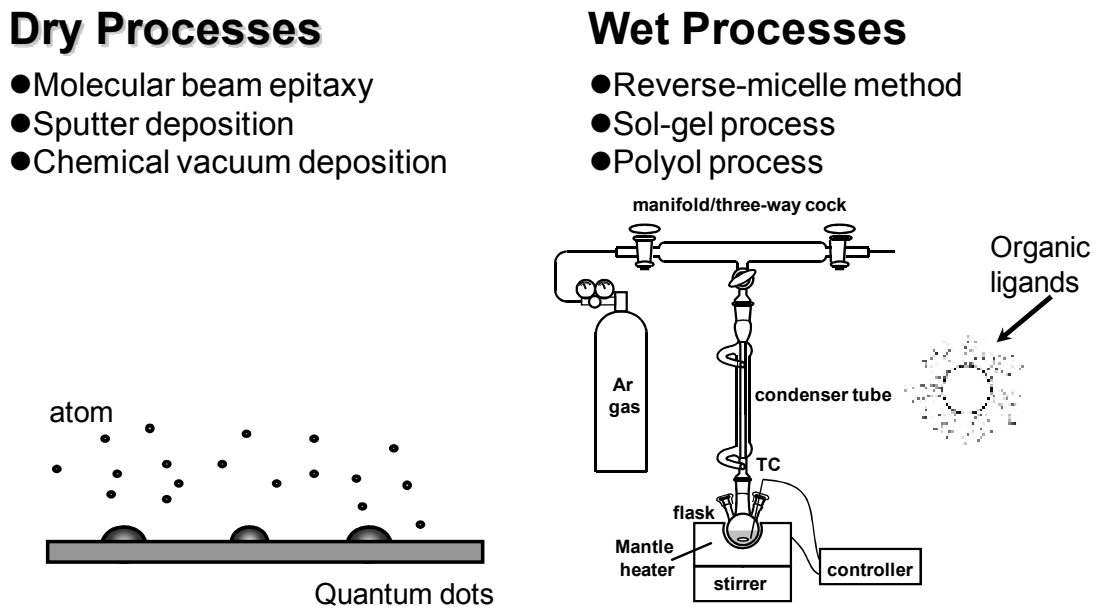

Figure 1.3 Schematic illustrations of synthesis methods of nanoparticles.

properties in the electron energy structure of the semiconductor nanoparticles provides the high photocatalytic activities and the highly efficiency photoluminescence compared to those of bulk materials.

So far various strategies for the preparation of nanoparticles have been reported, and they are roughly classified into two groups, chemical syntheses in solution phases (wet processes) and the preparation with physical techniques (dry processes) (Figure 1.3). In most cases preparation of nanoparticles in solution, the reduction of the corresponding metal ions or metal complexes is conducted in the presence of additional stabilizing agents e.g., thiol compounds and polymers.[1-31,48-69] As a result, the prepared suspension contains

byproducts, remaining substrates, and stabilizing agents. Since the species sometimes prevent utilization of the functionality of nanoparticles, their removal is inevitable. On the other hand, physical techniques such as metal vapor-deposition techniques enable the production of nanoparticles on solid substrates.[70-84] Though the obtained nanoparticles have a bare surface without adsorption of stabilizers, the amount of them is relatively small and their size distribution is generally broad.

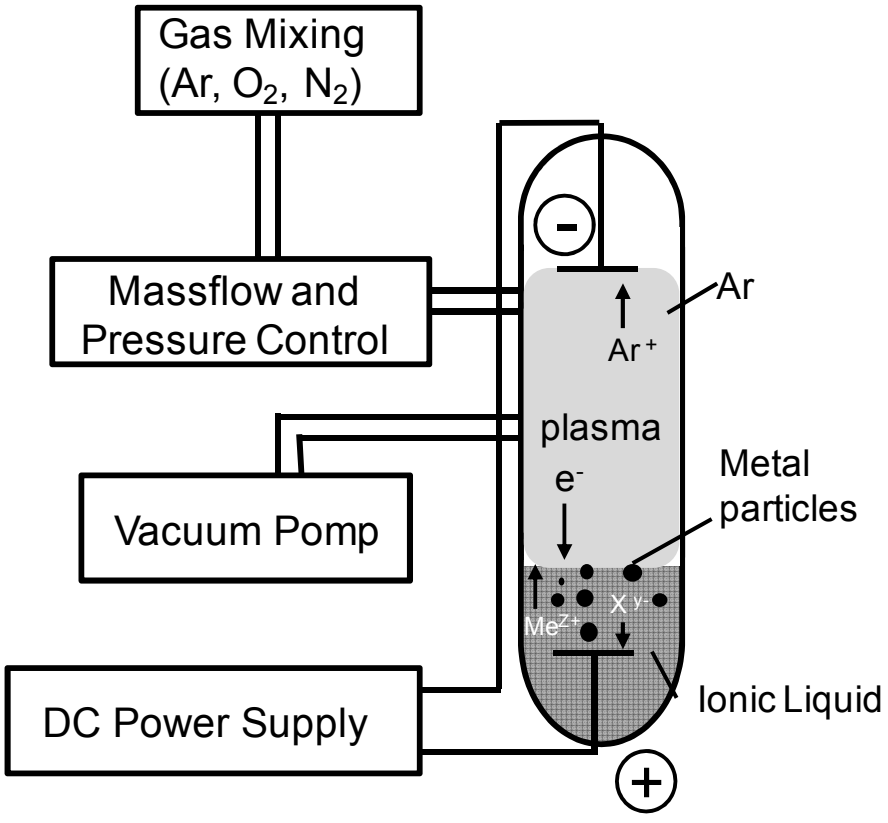

Figure1.4 Schematic illustration of the experimental setup for the plasma electrochemical reduction of metal ions dissolved in ILs.

Recently, novel preparation strategies have been developed for metal nanoparticles dispersed in organic solvents without formation of byproducts. For example, synthesis of metal nanoparticles was achieved by metal vacuum deposited on running liquid substrates of organic solvents having a very low vapor pressure, such as alkylnaphthalene and silicone oils.[85, 86] Stove et al. have developed the solvated metal atom deposition technique, where gold was vaporized under vacuum followed by deposition on the inside walls of a liquid-nitrogen-cooled vacuum chamber simultaneously with acetone vapor.[87] However, these methods required complicated apparatus equipped with rotary reactors or cooled traps to collect metal vapor, and furthermore, deposited nanoparticles generally made large aggregation unless suitable stabilizing agents, such as thiol compounds or surfactants.

Very recently, it has been reported an advanced method of the combination of physical techniques with ionic liquids (ILs) as a reaction medium enabled preparation of ultrafine metal nanoparticles uniformly dispersed in the solution.[88, 89] ILs have attractive features such as high ionic conductivity and capability to dissolve many kinds of substances.[90-92] Especially the extremely low vapor pressure of ILs has enabled the handing of ILs under a high vacuum condition, such as x-ray photoemission[93,94] and scanning electron spectroscopy.[95] ILs works also as stabilizer of the produced nanoparticles. It is not consequently required to add any capping molecules used for the conventional solvents.[96-106]

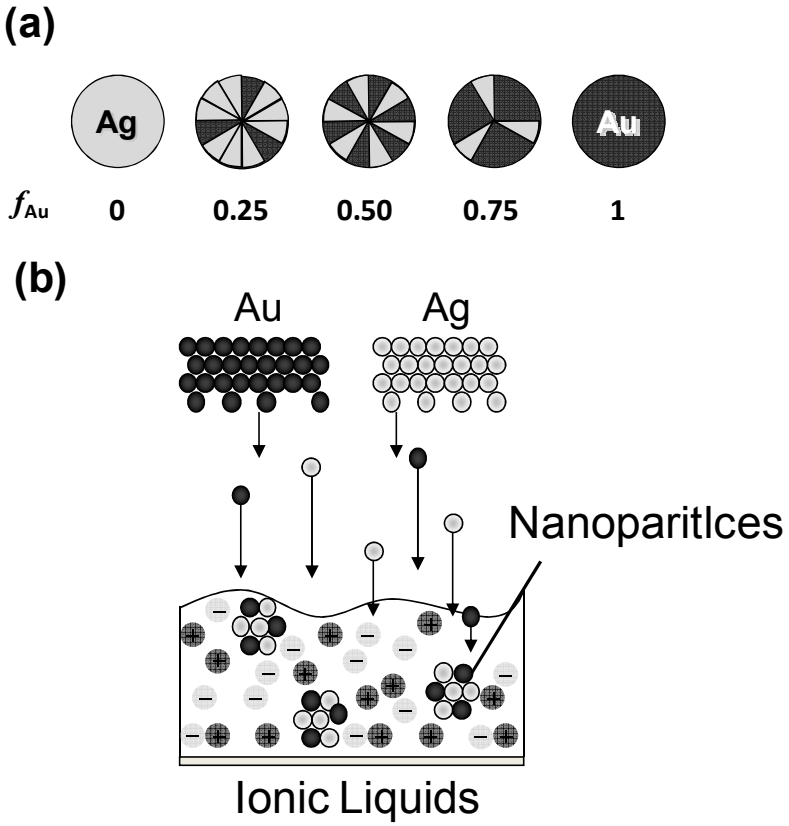

Figure 1.5 (a) Schematic illustrations of Au–Ag foil binary targets having various f_{Au}. (b) Schematic illustration of synthesis of the AuAg alloy nanoparticles by sputtering onto ionic liquids.

Endres and co-workers have reported the Ag nanoparticle synthesis in ILs using a glow discharge (plasma-electrochemical deposition) under reduced pressure conditions, in which metal ions dissolved in IL were reduced by Ar^+ plasma irradiation to produce the corresponding metal nanoparticles at interphase between IL and Ar^+ plasma (Figure 1.4).[101, 102] Torimoto et al, it has been reported that the sputtering of noble metal onto ILs produces the liquid containing highly dispersed metal nanoparticles, such as Au, Ag, and Pt.[103-112] The size of prepared nanoparticles was dependent on the kind of ILs used.[103] The sputter

deposition technique also enabled AuAg alloy nanoparticles with a desired composition by using Au and Ag binary metal target (Figure 1.5).[104]

1.2 Present study

Actually, the strategies have been limitedly applied to only noble metals. In this thesis, I have succeeded to extend their applications to other transition metals such as tungsten (W), molybdenum (Mo), niobium (Nb), and titanium (Ti) and indium (In). In addition, we applied this method to prepare alloy metals combined with the concept of liquid phase nanoparticle synthesis. My results propose a new strategy for preparation of metal and metal oxide nanoparticles with wide variety of composition and structures. I expect that the technique of sputter deposition into IL is one of the promising tools to discover novel advance nonmaterials.

Chapter 2 describes two topics; one is the influence of the sputtering conditions of Ag on nanoparticle's size and their size distribution in ILs, another utilization of their redox activities to prepare AuAg alloy nanoparticles directly in ILs. Sputter deposition of Ag onto IL produced Ag nanoparticles whose size was varied dependent on the sputtering conditions. Change in the discharge current from 10 to 40 mA increased Ag nanoparticles size from 5.7 to

11 nm, though prolongation of sputtering time simply caused a higher concentration of Ag nanoparticles in IL without any changes in their size. Sputter deposition of Ag onto IL containing $HAuCl_4$ resulted in the appearance of a single surface plasmon resonance peak in the absorption spectra of the resulting liquid, and their peak position was red-shifted with an increase in the concentration of $HAuCl_4$. The obtained results clearly indicated that Ag metal species sputter-deposited in IL can reduce $HAuCl_4$ to give AuAg alloy nanoparticles and that their chemical composition varied depending on the initial concentration of $HAuCl_4$.

Chapter 3 describes metal oxide nanoparticles synthesis in IL by sputtering the corresponding metal targets. Sputter deposition of transition metals W, Mo, Nb, and Ti onto IL produced corresponding metal oxide nanoparticles smaller than 6 nm, in which the oxidation of sputtered metal species occurred during the sputter deposition or on the exposure to the thus-obtained IL solutions to air. The obtained nanoparticles were composites composed of metal and metal oxide and were highly dispersed in IL without any additional stabilizing agents.

In Chapter 4, unique method to prepare the hollow nanoparticles of indium oxide could be fabricated by the oxidation of In metal nanoparticles in ILs is described. Sputter deposition of In in IL produced stable metal nanoparticles of In whose surfaces were covered by an amorphous In_2O_3 layer, forming In/In_2O_3 core/shell structure. The size of the In core

was tunable from ca.8 to 20 nm by selecting the kind of IL, whereas the shell thickness of In_2O_3 was almost constant at ca.1.9 nm. Heat treatment of the thus-obtained nanoparticles at 523K in air oxidized In metal of the core, resulting in the formation of spherical hollow nanoparticles made of crystalline In_2O_3. The size of the hollow nanoparticles was slightly larger than that of the In/In_2O_3 core/shell nanoparticles used as a starting material, whereas the void space formed inside hollow nanoparticles was smaller than the corresponding In metal cores. These facts indicated that in addition to the predominant outward diffusion of In ions, an inward transport of oxygen ions occurred, and thus an In_2O_3 crystal could be grown on both the inner concave and outer convex surfaces of the oxide shell layer.

Finally, Chapter 5 describes general remarks on this thesis, summarizing my novel findings through the researches and expected future contributions to the future nanoparticle sciences and engineering.

1.3 References

(1) Torimoto, T.; Adachi, T.; Okazaki, K.; Sakuraoka, M.; Shibayama, T.; Ohtani, B.; Kudo, A.; Kuwabata, S., *J. Am. Chem. Soc*. **2007**, 129, 12388.

(2) Shen, Z. R.; Yamada, M.; Miyake, M., *Chem. Commun.***2007**, 245.

(3) Li, P.; Nan, C. Y.; Wei, Z.; Lu, J.; Peng, Q.; Li, Y. D., *Chem. Mater.* **2010**, 22, 4232.

(4) Yang, J.; Lee, J. Y.; Too, H. P., *J. Phys. Chem. B* **2005**, 109, 19208.

(5) Kikuchi, E.; Kitada, S.; Ohno, A.; Aramaki, S.; Maenosono, S., *Appl. Phys. Lett* **2008**, 92, 173307.

(6) Teranishi, T.; Sugawara, A.; Shimizu, T.; Miyake, M., *J. Am. Chem. Soc*. **2002**, 124, 4210.

(7) Shevchenko, E. V.; Talapin, D. V.; Schnablegger, H.; Kornowski, A.; Festin, O.; Svedlindh, P.; Haase, M.; Weller, H., *J. Am. Chem. Soc*. **2003,** 125, 9090.

(8) Shen, Z.; Yamada, M.; Miyake, M., *J. Am. Chem. Soc*. **2007**, 129, 14271.

(9) Hills, C. W.; Nashner, M. S.; Frenkel, A. I.; Shapley, J. R.; Nuzzo, R. G., *Langmuir* **1999**, 15, 690.

(10) Sun, S. H.; Murray, C. B.; Weller, D.; Folks, L.; Moser, A., *Science* **2000**, 287, 989.

(11) Ahmadi, T. S.; Wang, Z. L.; Green, T. C.; Henglein, A.; ElSayed, M. A., *Science* **1996**, 272, 1924.

(12) Brust, M.; Fink, J.; Bethell, D.; Schiffrin, D. J.; Kiely, C., *J. Chem. Soc., Chem. Commun.* **1995**, 1655.

(13) Brust, M.; Walker, M.; Bethell, D.; Schiffrin, D. J.; Whyman, R., *J. Chem. Soc., Chem. Commun.* **1994**, 801.

(14) Crooks, R. M.; Zhao, M. Q.; Sun, L.; Chechik, V.; Yeung, L. K., *Acc. Chem. Res.* **2001**, 34, 181.

(15) Daniel, M. C.; Astruc, D., G *Chem. Rev.* **2004**, 104, 293.

(16) Gupta, A. K.; Gupta, M., *Biomaterials* **2005**, 26, 3995.

(17) Hyeon, T., *Chem. Commun.* **2003**, 927.

(18) Hyeon, T.; Lee, S. S.; Park, J.; *J. Am. Chem. Soc*. **2001**, 123, 12798.

(19) Jana, N. R.; Gearheart, L.; Murphy, C. J., *Adv. Mater*. **2001**, 13, 1389.

(20) Katz, E.; Willner, I., *Angew. Chem. Int. Edit.* **2004**, 43, 6042.

(21) Li, M.; Schnablegger, H.; Mann, S., *Nature* **1999**, 402, 393.

(22) Lu, A. H.; Salabas, E. L.; Schuth, F., *Angew. Chem. Int. Edit.* **2007**, 46, 1222.

(23) Meulenkamp, E. A., *J. Phys. Chem. B* **1998**, 102, 5566.

(24) Michalet, X.; Pinaud, F. F.; Bentolila, L. A.; Tsay, J. M.; Doose, S.; Li, J. J.; Sundaresan, G.; Wu, A. M.; Gambhir, S. S.; Weiss, S., *Science* **2005**, 307, 538.

(25) Murphy, C. J.; San, T. K.; Gole, A. M.; Orendorff, C. J.; Gao, J. X.; Gou, L.; Hunyadi, S.

E.; Li, T., *J. Phys. Chem. B* **2005**, 109, 13857.

(26) Raveendran, P.; Fu, J.; Wallen, S. L., *J. Am. Chem. Soc*. **2003**, 125, 13940.

(27) Sau, T. K.; Murphy, C. J., *J. Am. Chem. Soc*. **2004**, 126, 8648.

(28) Scott, R. W. J.; Wilson, O. M.; Crooks, R. M., *J. Phys. Chem. B* **2005**, 109, 692.

(29) Suenaga, K.; Colliex, C.; Demoncy, N.; Loiseau, A.; Pascard, H.; Willaime, F., *Science* **1997**, 278, 653.

(30) Sun, Y. G.; Xia, Y. N., *Science* **2002**, 298, 2176.

(31) Taleb, A.; Petit, C.; Pileni, M. P., *Chem. Mater.* **1997**, 9, 950.

(32) Kongkanand, A.; Kuwabata, S.; Girishkumar, G.; Kamat, P., *Langmuir* **2006**, 22, 2392.

(33) Haruta, A., *Chemical Record* **2003**, 3, 75.

(34) Kelly, K. L.; Coronado, E.; Zhao, L. L.; Schatz, G. C., *J. Phys. Chem. B* **2003**, 107, 668.

(35) Haynes, C. L.; Van Duyne, R. P., *J. Phys. Chem. B* **2001**, 105, 5599.

(36) Haes, A. J.; Van Duyne, R. P., *J. Am. Chem. Soc*. **2002**, 124, 10596.

(37) Hutter, E.; Fendler, J. H., *Adv. Mater*. **2004**, 16, 1685.

(38) Malinsky, M. D.; Kelly, K. L.; Schatz, G. C.; Van Duyne, R. P., *J. Am. Chem. Soc*. **2001**, 123, 1471.

(39) Willets, K. A.; Van Duyne, R. P., *Annu. Rev. Phys. Chem.* **2007**, 58, 267.

(40) Jain, P. K.; Huang, W. Y.; El-Sayed, M. A., *Nano Lett.* **2007**, 7, 2080.

(41) Anker, J. N.; Hall, W. P.; Lyandres, O.; Shah, N. C.; Zhao, J.; Van Duyne, R. P., *Nature Mater.* **2008**, 7, 442.

(42) Haes, A. J.; Hall, W. P.; Chang, L.; Klein, W. L.; Van Duyne, R. P., *Nano Lett.* **2004**, 4, 1029.

(43) Haes, A. J.; Van Duyne, R. P., *Anal. Bioanal Chem.* **2004**, 379, 920.

(44) McFarland, A. D.; Young, M. A.; Dieringer, J. A.; Van Duyne, R. P., *J. Phys. Chem. B* **2005**, 109, 11279.

(45) Barnes, W. L.; Dereux, A.; Ebbesen, T. W., *Nature* **2003**, 424, 824.

(46) Liu, Z. X.; Song, H. W.; Zheng, Z. H.; Lu, S. Z.; Yu, L. X.; Yang, L. M., *Colloid. Surf. Phys. Eng. Aspects* **2006**, 275, 69.

(47) Ueno, K.; Juodkazis, S.; Shibuya, T.; Yokota, Y.; Mizeikis, V.; Sasaki, K.; Misawa, H., *J. Am. Chem. Soc*. **2008**, 130, 6928.

(48) Henglein, A., *Chem. Rev.* **1989**, 89, 1861.

(49) Bawendi, M. G.; Steigerwald, M. L.; Brus, L. E., *Annu. Rev. of Phys. Chem.* **1990**, 41, 477.

(50) Wang, Y.; Herron, N., *J. Phys. Chem.* **1991**, 95, 525.

(51) Kamat, P. V., *Chem. Rev.* **1993**, 93, 267.

(52) Weller, H., *Angew. Chem. Int. Edit.* **1993**, 32, 41.

(53) Hagfeldt, A.; Gratzel, M., *Chem. Rev.* **1995**, 95, 49.

(54) Alivisatos, A. P., *J. Phys. Chem.* **1996**, 100, 13226.

(55) Vossmeyer, T.; Katsikas, L.; Giersig, M.; Popovic, I. G.; Diesner, K.; Chemseddine, A.; Eychmuller, A.; Weller, H., *J. Phys. Chem.* **1994**, 98, 7665.

(56) Park, J.; Joo, J.; Kwon, S. G.; Jang, Y.; Hyeon, T., *Angew. Chem. Int. Edit.***2007**, 46, 4630.

(57) Murray, C. B.; Norris, D. J.; Bawendi, M. G., *J. Am. Chem. Soc*. **1993**, 115, 8706.

(58) Dabbousi, B. O.; RodriguezViejo, J.; Mikulec, F. V.; Heine, J. R.; Mattoussi, H.; Ober, R.; Jensen, K. F.; Bawendi, M. G., *J. Phys. Chem. B* **1997**, 101, 9463.

(59) Duan, X. F.; Lieber, C. M., *Adv. Mater*. **2000**, 12, 298.

(60) Hines, M. A.; Guyot-Sionnest, P., *J. Phys. Chem.* **1996**, 100, 468.

(61) Hostetler, M. J.; Wingate, J. E.; Zhong, C. J.; Harris, J. E.; Vachet, R. W.; Clark, M. R.; Londono, J. D.; Green, S. J.; Stokes, J. J.; Wignall, G. D.; Glish, G. L.; Porter, M. D.; Evans, N. D.; Murray, R. W., *Langmuir* **1998**, 14, 17.

(62) Joo, S. H.; Choi, S. J.; Oh, I.; Kwak, J.; Liu, Z.; Terasaki, O.; Ryoo, R., *Nature* **2001**, 412, 169.

(63) Manna, L.; Scher, E. C.; Alivisatos, A. P., *J. Am. Chem. Soc*. **2000**, 122, 12700.

(64) Morales, A. M.; Lieber, C. M., *Science* **1998**, 279, 208.

(65) Murray, C. B.; Kagan, C. R.; Bawendi, M. G., *Ann. Rev. Mat. Sci*. **2000**, 30, 545.

(66) Peng, X. G.; Schlamp, M. C.; Kadavanich, A. V.; Alivisatos, A. P., *J. Am. Chem. Soc*. **1997**, 119, 7019.

(67) Puntes, V. F.; Krishnan, K. M.; Alivisatos, A. P., *Science* **2001**, 291, 2115.

(68) Vayssieres, L., *Adv. Mater*. **2003**, 15, 464.

(69) Xia, Y. N.; Yang, P. D.; Sun, Y. G.; Wu, Y. Y.; Mayers, B.; Gates, B.; Yin, Y. D.; Kim, F.; Yan, Y. Q., *Adv. Mater*. **2003**, 15, 353.

(70) Banerjee, A. N.; Chattopadhyay, K. K., *J. Appl. Phys* **2005**, 97, 084308.

(71) Brown, E. R.; Bacher, A.; Driscoll, D.; Hanson, M.; Kadow, C.; Gossard, A. C., *Phy. Rev. Lett.* **2003**, 90,077403

(72) Dvurechenskii, A. V.; Smagina, J. V.; Groetzschel, R.; Zinovyev, V. A.; Armbrister, V. A.; Novikov, P. L.; Teys, S. A.; Gutakovskii, A. K., *Surf. Coat. Tech.* **2005**, 196, 25.

(73) Eisenhammer, T.; Trampert, A., *Phy. Rev. Lett.* **1997**, 78, 262.

(74) Goebbert, C.; Nonninger, R.; Aegerter, M. A.; Schmidt, H., *Thin Solid Films* **1999**, 351, 79.

(75) Hao, Y. F.; Meng, G. W.; Ye, C. H.; Zhang, L. D., *Cryst. Growth Des.* **2005**, 5, 1617.

(76) Okumu, J.; Dahmen, C.; Sprafke, A. N.; Luysberg, M.; von Plessen, G.; Wuttig, M., *J. Appl. Phys* **2005**, 97, 094305.

(77) Okumura, M.; Nakamura, S.; Tsubota, S.; Nakamura, T.; Azuma, M.; Haruta, M., *Catal. Lett.* **1998**, 51, 53.

(78) Okumura, M.; Tsubota, S.; Iwamoto, M.; Haruta, M., *Chem. Lett.* **1998**, 27, 315.

(79) Patella, F.; Fanfoni, M.; Arciprete, F.; Nufris, S.; Placidi, E.; Balzarotti, A., *Appl. Phys. Lett.* **2001**, 78, 320.

(80) Tsantilis, S.; Kammler, H. K.; Pratsinis, S. E., *Chem. Eng. Sci.* **2002**, 57, 2139.

(81) Wu, W. Y.; Ting, J. M., *Thin Solid Films* **2002**, 420, 166.

(82) Wu, Y.; Chen, Q.; Takeguchi, M.; Furuya, K., *Surf. Sci*. **2000**, 462, 203.

(83) Xiu, Y. H.; Zhu, L. B.; Hess, D. W.; Wong, C. P., *Langmuir* **2006**, 22, 9676.

(84) Zacharia, R.; Rather, S. U.; Hwang, S. W.; Nahm, K. S., *Chem. Phy. Lett.* **2007**, 434, 286.

(85) Nakatani, I.; Furubayashi, T.; Takahashi, T.; Hanaoka, H., *J. Magn. Magn. Mater* **1987**, 65, 261.

(86) Wagener, M.; Gunther, B., *J. Magn. Magn. Mater* **1999**, 201, 41.

(87) Stoeva, S.; Klabunde, K. J.; Sorensen, C. M.; Dragieva, I., *J. Am. Chem. Soc*. **2002**, 124, 2305.

(88) Tsuda, T.; Seino, S.; Kuwabata, S., *Chem. Commun.* **2009**, 6792.

(89) Imanishi, A.; Tamura, M.; Kuwabata, S., *Chem. Commun.* **2009**, 1775.

(90) Welton, T., *Chem. Rev.* **1999**, 99, 2071.

(91) Antonietti, M.; Kuang, D. B.; Smarsly, B.; Yong, Z., *Angew. Chem. Int. Edit.* **2004**, 43, 4988.

(92) Earle, M. J.; Esperanca, J.; Gilea, M. A.; Lopes, J. N. C.; Rebelo, L. P. N.; Magee, J. W.; Seddon, K. R.; Widegren, J. A., *Nature* **2006**, 439, 831.

(93) Smith, E. F.; Villar Garcia, I. J.; Briggs, D.; Licence, P., *Chem. Commun.* **2005**, 5633.

(94) Smith, E. F.; Rutten, F. J. M.; Villar-Garcia, I. J.; Briggs, D.; Licence, P., *Langmuir* **2006**, 22, 9386.

(95) Kuwabata, S.; Kongkanand, A.; Oyamatsu, D.; Torimoto, T., *Chem. Lett.* **2006**, 35, 600.

(96) Migowski, P.; Dupont, J., *Chem.Eur. J.* **2007**, 13, 32.

(97) Parvulescu, V. I.; Hardacre, C., *Chem. Rev.* **2007**, 107, 2615.

(98) Ott, L. S.; Finke, R. G., Coordination *Chem. Rev.* **2007**, 251, 1075.

(99) Redel, E.; Thomann, R.; Janiak, C., *Inorganic Chemistry* **2008**, 47, 14.

(100) Dash, P.; Dehm, N. A.; Scott, R. W. J., *J. Mol. Catal. Chem.* **2008**, 286, 114.

(101) Meiss, S. A.; Rohnke, M.; Kienle, L.; El Abedin, S. Z.; Endres, F.; Janek, J., *Chemphyschem* **2007**, 8, 50.

(102) El Abedin, S. Z.; Polleth, M.; Meiss, S. A.; Janek, J.; Endres, F., *Green Chem.* **2007**, 9, 549.

(103) Torimoto, T.; Okazaki, K.; Kiyama, T.; Hirahara, K.; Tanaka, N.; Kuwabata, S., *Appl. Phys. Lett.* **2006**, 89, 243117.

(104) Okazaki, K. I.; Kiyama, T.; Hirahara, K.; Tanaka, N.; Kuwabata, S.; Torimoto, T., *Chem. Commun.* **2008**, 691.

(105) Okazaki, K.; Kiyama, T.; Suzuki, T.; Kuwabata, S.; Torimoto, T., *Chem. Lett.* **2009**, 38, 330.

(106) Khatri, O. P.; Adachi, K.; Murase, K.; Okazaki, K.; Torimoto, T.; Tanaka, N.; Kuwabata, S.; Sugimura, H., *Langmuir* **2008**, 24, 7785.

(107) Tsuda, T.; Kurihara, T.; Hoshino, Y.; Kiyama, T.; Okazaki, K.; Torimoto, T.; Kuwabata, S., *Electrochemistry* **2009**, 77, 693.

(108) Kameyama, T.; Ohno, Y.; Kurimoto, T.; Okazaki, K.; Uematsu, T.; Kuwabata, S.; Torimoto, T., *Phys. Chem. Chem. Phy.* **2010**, 12, 1804.

(109) Tsuda, T.; Yoshii, K.; Torimoto, T.; Kuwabata, S., *J. Power Sources* **2010**, 195, 5980.

(110) Oda, Y.; Hirano, K.; Yoshii, K.; Kuwabata, S.; Torimoto, T.; Miura M. *Chem. Lett.* **2010**, 39, 1069.

(111) Torimoto, T.; Tsuda, T.; Okazaki, K.; Kuwabata, S., *Adv. Mater*. **2010**, 22, 1196.

(112) Kuwabata, S.; Tsuda, T.; Torimoto, T., *J. Phys. Chem. Lett.* **2010**, 1, 3177.

Chapter 2

Synthesis of AuAg Alloy Nanoparticles Using a Chemical Reaction Induced by Sputter Deposition of Metal onto Ionic Liquids

2.1 Introduction

Metal nanoparticles have been attractive materials for applications such as biosensors, catalysts and optoelectronic devices, because they exhibit unique physicochemical properties distinct from those of pure monometallic nanoparticles, being dependent on the size, shape, and composition of nanoparticles.[1-5] Ionic liquids (ILs) have been promising solvents for various reactions such as organic[6,7] and inorganic[8,9] syntheses and electrochemical reactions.[10,11] Preparation of metal nanoparticles has attracted much attention because they could catalyze unique reactions in ILs that did not occur in conventional organic or aqueous solvents. Several strategies have been developed for the preparation of metal nanoparticles, such as Pt,[12] Rh,[12] Ir,[13] and Au,[14] uniformly dispersed in ILs. Torimoto et al. has recently developed a method to prepare metal nanoparticles in ILs without any additives, such as reducing agents and/or stabilizing agents. The extremely low vapor pressure of ILs enabled sputter deposition of metal species onto ILs under vacuum, resulting in the formation of

highly dispersed metal nanoparticles, such as Au, Ag and Pt, having sizes of 2～5 nm.[15-24] Furthermore, it has been reported that injection of low-energy electrons into ILs induced the reduction of metal ions, such as Ag^{+}[25,26] and $AuCl_4^{-}$,[27] to produce corresponding metal particles. If metal nanoparticles having an oxidation potential were sputter-deposited in IL containing another metal ions having more positive reduction potential, the latter metal ions could be reduced to form nanoparticles. However, such an attempt has never been made.

In this chapter, I prepared Ag nanoparticles having various sizes by sputter-deposition onto an IL with different conditions. Furthermore, Ag-sputtering was made onto IL solutions containing $HAuCl_4$ to produce AuAg alloy nanoparticles.

2.2 Experimental Section

2.2.1 Materials

1-butyl-3-methylimidazolium hexafluorophosphate (BMI-PF_6) was purchased from Kanto Chemical.1,6-hexanedithiol was purchased from Tokyo Chemical Industry. Acetonitrile and $HAuCl_4$ were purchased from Kishida Reagents Chemicals.

2.2.2 Synthesis of Ag nanoparticles by sputter deposition onto ionic liquids.

The IL (BMI-PF_6) was dried for 3 h at 393 K under vacuum just before use. Sputter deposition of silver in IL was performed using a sputter coater (Sanyu Electron Co., Ltd, SC-701HMCII) with various sputtering condition under argon (> 99.99%) pressure at room temperature. An IL (0.60 cm^3) was spread on a glass plate (10 cm^2) that was horizontally set in the sputter coater. The surface of the IL was located at distances of 85 mm from the silver foil target (99.99% in purity). The sputtering was carried out for various times.

2.2.3 Synthesis of AuAg alloy nanoparticles using a chemical reaction induced by sputter deposition of metal onto ionic liquids.

A portion of $HAuCl_4$ ethanol solution was added to BMI-PF_6, followed by drying for 3 h at 378 K under vacuum. A 0.60 cm^3 portion of thus-obtained solution was spread on a glass plate (10 cm^2) that was horizontally set in the sputter coater(Sanyu Electron Co., Ltd, SC-701HMCII). The surface of the IL was located at a distance of 85 mm from the silver foil target (99.99% in purity). The sputtering was carried out for 5 min under 5.0 Pa of argon gas with 10mA of ion current. .

2.2.4 Characterization of nanoparticles.

The structure and size of nanoparticles formed in IL were observed using a transmission electron microscope (TEM; HITACHI H-7650) operated at an acceleration voltage of 100 kV. Samples for TEM measurements were prepared by dropping an IL solution containing nanoparticles onto a copper grid with amorphous carbon overlayers (Oken Shoji, #10-1012), followed by removal of the excess amount of solution with a filter paper.

The concentration of Ag deposited in IL was determined by using X-ray fluorescence spectrometer (XRF; Rigaku EDXL300). A 0.2 cm^3 portion of Ag nanoparticle IL solution was mixed with 1.0 cm^3 methanol solution containing 1,6-hexanedithiol (0.05 cm^3), followed by the centrifugation. Thus-obtained precipitates of Ag nanoparticles were dissolved in a HNO_3 aqueous solution and then subjected to the XRF analysis.

For the preparation of XPS samples, metal nanoparticles dispersed in IL were isolated by precipitation with addition of a small amount of acetonitrile to BMI-PF_6 solution, washed with acetonitrile several times, and dispersed in acetonitrile. Elemental composition of isolated AuAg alloy nanoparticles was examined with X-ray photoelectron spectroscopy (XPS; JEOL JPS-9000MC), by considering peak areas of each band in XPS spectra and their corresponding relative sensitivity factor.

2.3 Results and Discussion

2.3.1 Size control of nanoparticles by sputter conditions

Figure 2.1 (a) shows changes in the absorption spectra of BMI-PF_6 by sputter deposition of Ag with various sputtering times. A sharp absorption peak at ca. 420 nm that developed with elapse of sputtering time was assigned to the surface plasmon resonance (SPR) peak of Ag nanoparticles. The concentration of Ag linearly increased from 0.26 to 2.4 mmol dm^{-3} with sputtering time from 5 to 45 min (Fig. 2.1 (b)). TEM observation revealed that the spherical Ag nanoparticles with a size of ca. 5.7 nm were formed regardless of sputtering time. Similar behavior was observed for Au sputter deposition in our previous study.[16]

On the other hand, as shown in Figure 2.1 (c), the SPR peak intensity of Ag nanoparticles increased with an increase in discharge current from 10 to 40 mA, resulting in an increase in the concentration of Ag from 0.26 to 1.4 mmol dm^{-3}. The size of nanoparticles formed also increased from 5.7 to 11 nm with an increase in discharge current from 10 to 40 mA. In sputter deposition, bombardment of energetic gaseous ions on the Ag foil surface causes physical ejection of surface atoms and/or clusters, which are injected into the IL solution. The density of these Ag species at the solution surface became high enough

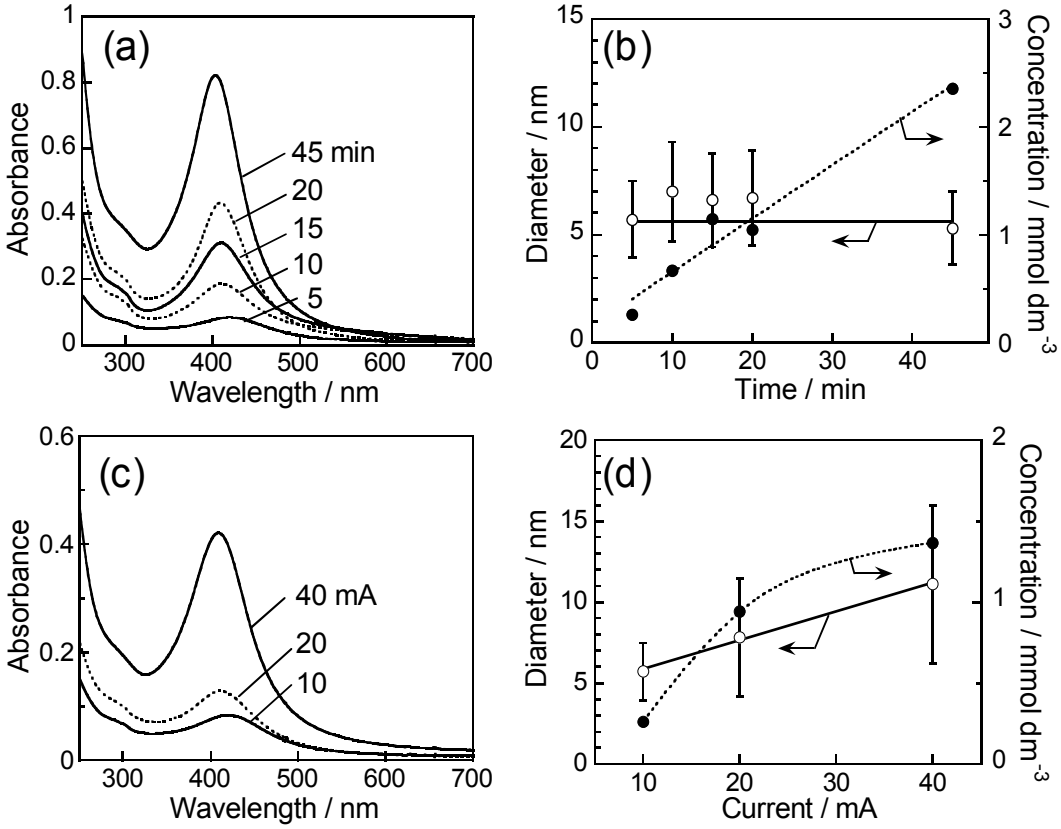

Figure 2.1 Absorption spectra obtained after Ag sputter deposition (a, c) and dependence of average size (open circles) and concentration (solid circles) of the thus-obtained Ag nanoparticles on sputtering conditions (b, d). A constant discharge current of 10 mA was used (a, b) or the sputtering time was fixed to 5 min (c, d). The optical length of a quartz cuvette used was 1.0 mm. The numbers in figures represent the sputtering time (a) or the discharge current (c). The error bars in figure b and d indicate the size distribution.

to coalesce with each other, the degree being remarkable with high discharge current. The coalescence of sputtered species proceeds until Ag nanoparticles have been stabilized by the adsorption of ions of the IL.

2.3.2 Alloy nanoparticles prepared with sputter-deposition of metal onto ionic liquids and chemical reaction in solution

Figure 2.2(a) shows absorption spectra of BMI-PF_6 containing $HAuCl_4$ after sputter deposition of Ag. A single SPR peak is observed in each spectrum. The peak shape became broad and then the peak wavelength (λ_{SPR}) was red-shifted with an increase in $HAuCl_4$ concentration (Figure 2.2(b)). It has been reported by Xia and coworkers that $AuCl_4^-$ ions in aqueous solutions were reduced by oxidative dissolution of Ag metal, according to eq.2.1, resulting in AuAg alloy formation of nanoparticles or hollow shells. [31,32]

$$AuCl_4^- + 3Ag = Au + 3AgCl + Cl^- \text{ ---------- (2.1)}$$

In this case also, it seems reasonable that AuAg alloy nanoparticles in BMI-PF_6 were formed by the reduction of $HAuCl_4$ with sputter-deposited Ag species because it has been reported that AuAg alloy nanoparticles exhibited a single SPR peak in absorption spectra whose wavelength was linearly red-shifted with an increase in the fraction of Au atoms in the nanoparticles.[33] It was confirmed by TEM and XPS that the chemical composition of AuAg alloy nanoparticles was changed by changing the concentration of $HAuCl_4$ in BMI-PF_6.

Alloy nanoparticles were isolated by the addition of acetonitrile to IL solutions. TEM observation of these nanoparticles revealed that solid spherical nanoparticles were formed in BMI-PF_6 solutions by sputter deposition of Ag, regardless of the concentration of $HAuCl_4$, as shown in Figure 2.3. The size determined from TEM measurements increased slightly with an increase in the initial concentration of $HAuCl_4$: the Ag nanoparticles sputter-deposited in pure BMI-PF_6 had an average diameter (d_{av}) of 5.7 nm with a standard deviation (σ) of 1.8 nm, while sputter deposition onto solutions containing 65 and 100 μmol dm^{-3} $HAuCl_4$ produced nanoparticles having d_{av} (σ) of 6.4 (2.6) and 6.9 (2.9) nm, respectively. A little larger values of d_{av} and σ for AuAg alloy nanoparticles than those for Ag nanoparticles is due probably to progress of some aggregation during Ag oxidation and Au deposition reactions. However, the prepared AuAg nanoparticles were stable for several days without change in their absorption spectra.

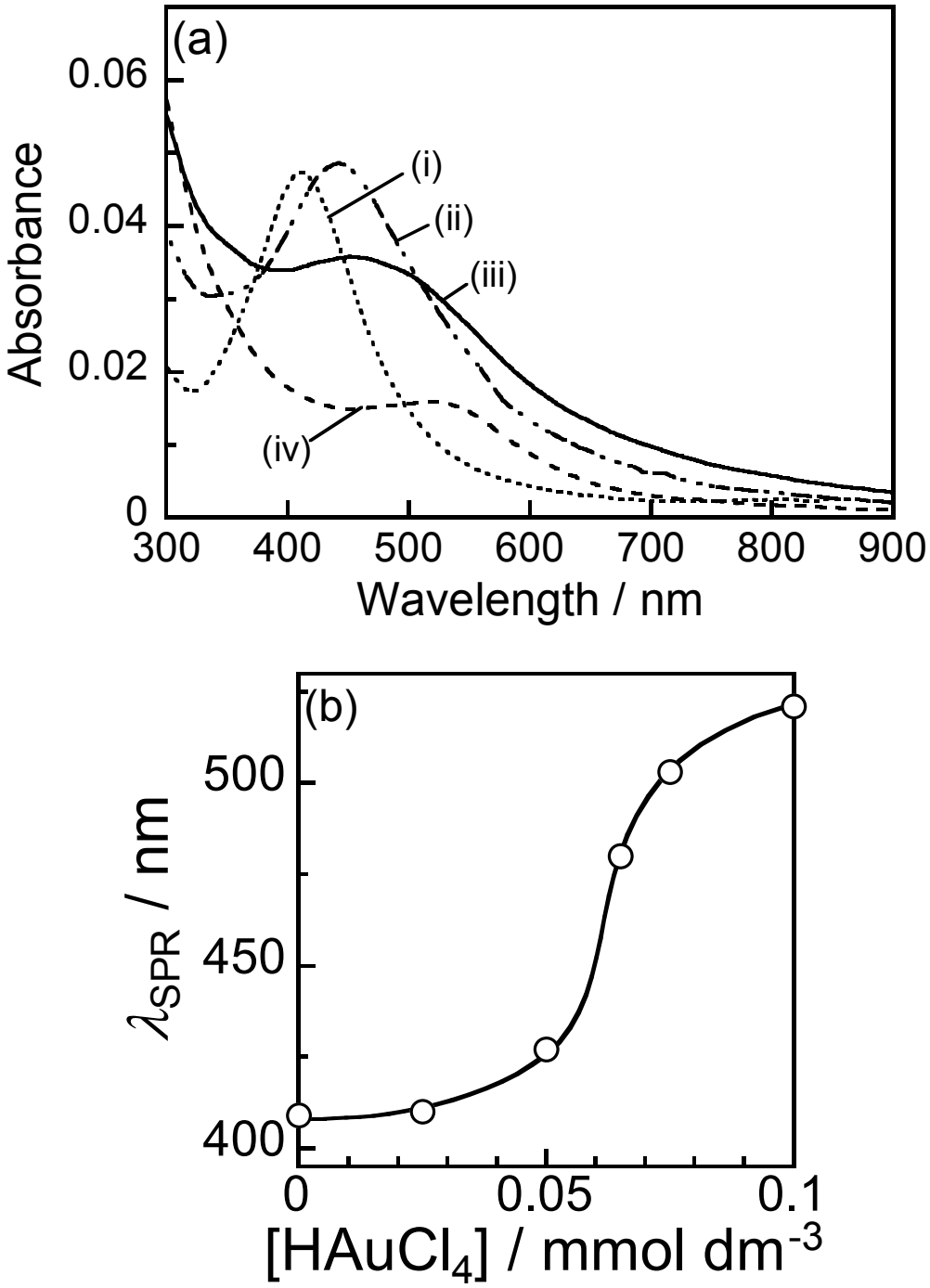

Figure 2.2 **(a)** Absorption spectra of BMI-PF_6 solutions after sputter deposition of Ag. The initial concentrations of $HAuCl_4$ were 0 (i), 50 (ii), 65 (iii), and 100 μmol dm^{-3}(iv). The optical length of a quartz cuvette used was 1.0 mm. (b) The SPR peak wavelengths are plotted as a function of the initial concentration of $HAuCl_4$. Sputter deposition of Ag onto ILs was carried out for 5 min with a discharge current of 10 mA.

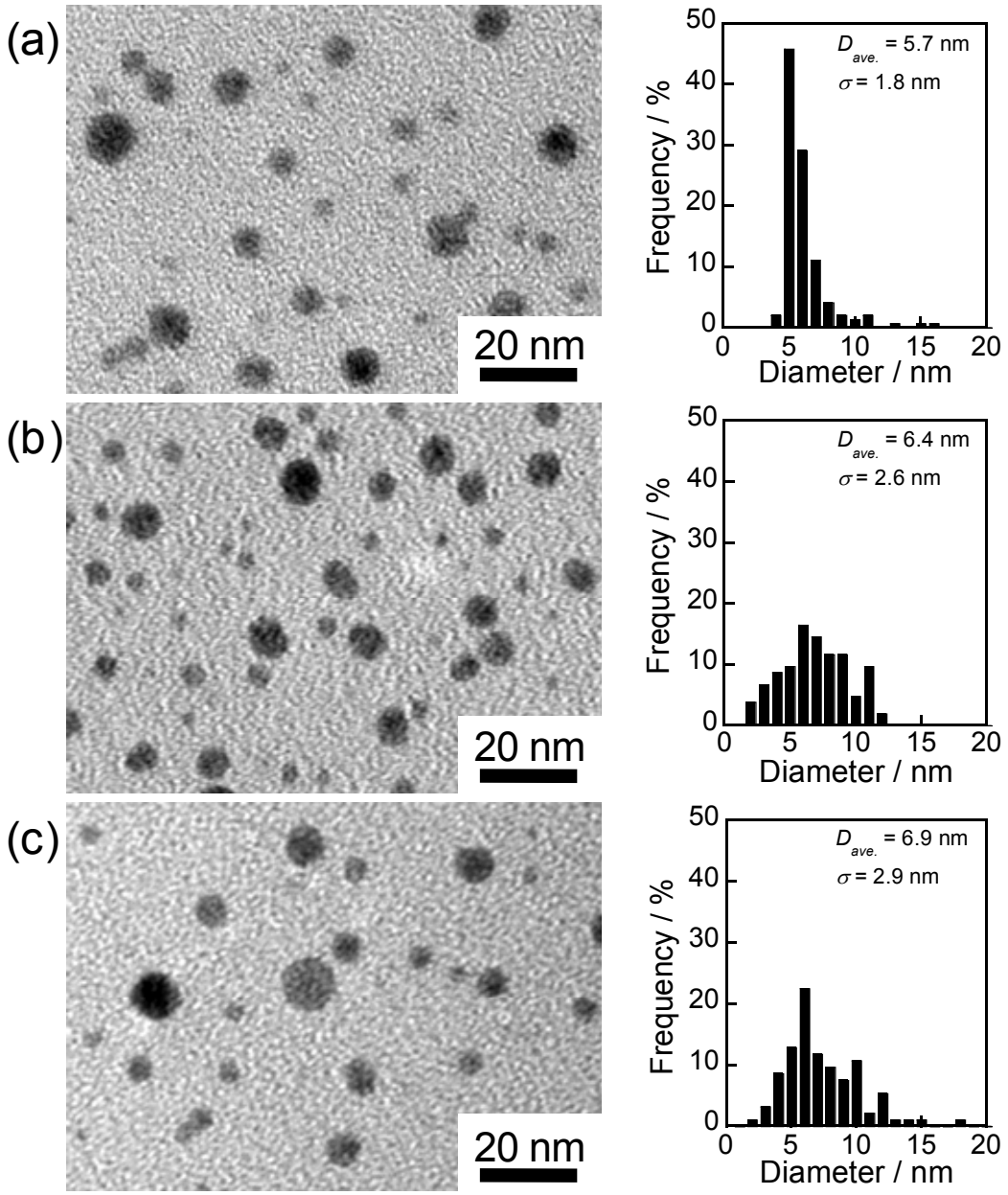

Figure 2.3 TEM images of Ag nanoparticles sputter-deposited in pure BMI-PF_6 (a) and AuAg nanoparticles prepared in BMI-PF_6 containing 65 (b) and 100 (c) μmol dm^{-3} $HAuCl_4$. Size distributions are also shown on the right side of the corresponding TEM images.

XPS spectra of AuAg nanoparticles isolated from BMI-PF_6 containing 65 μmol dm^{-3} $HAuCl_4$ showed that the binding energies of Au $4f_{7/2}$ and Au $4f_{5/2}$ appeared at 83.1 and 86.8 eV and those of Ag $3d_{5/2}$ and Ag $3d_{3/2}$ appeared at 367.3 and 373.3 eV, respectively (Figure 2.4(a) and 2.4(b)). The energies for gold and silver were in good agreement with the literature values reported for AuAg alloy nanoparticles.[34] Since no signals assigned to Cl atoms were detected (Figure 2.4(c)), AgCl particles were not contained in the particles isolated from IL solutions. These facts suggest that AgCl particles are extremely small even if they are formed according to eq.2.1, and then the simple addition of acetonitrile to IL solutions can not cause the precipitation of AgCl under the conditions used in the present study. The present sputtering conditions have to give 260 μmol dm^{-3} Ag concentration in the BMI-PF_6 solutions. Therefore, according to eq.2.1, alloy nanoparticles formed in solutions containing $HAuCl_4$ of 65 and 100 μmol dm^{-3} are expected to form AuAg alloy with Au/Ag ratios of 50/50 and 100/0, respectively. However, XPS analyses revealed the ratios of 34/66 and 90/10, respectively. These facts suggest that all sputtered Ag atoms did not react with $HAuCl_4$ in the solutions. It is likely that the formation of Au-rich alloy shells retards the oxidative dissolution of Ag nanoparticle cores.

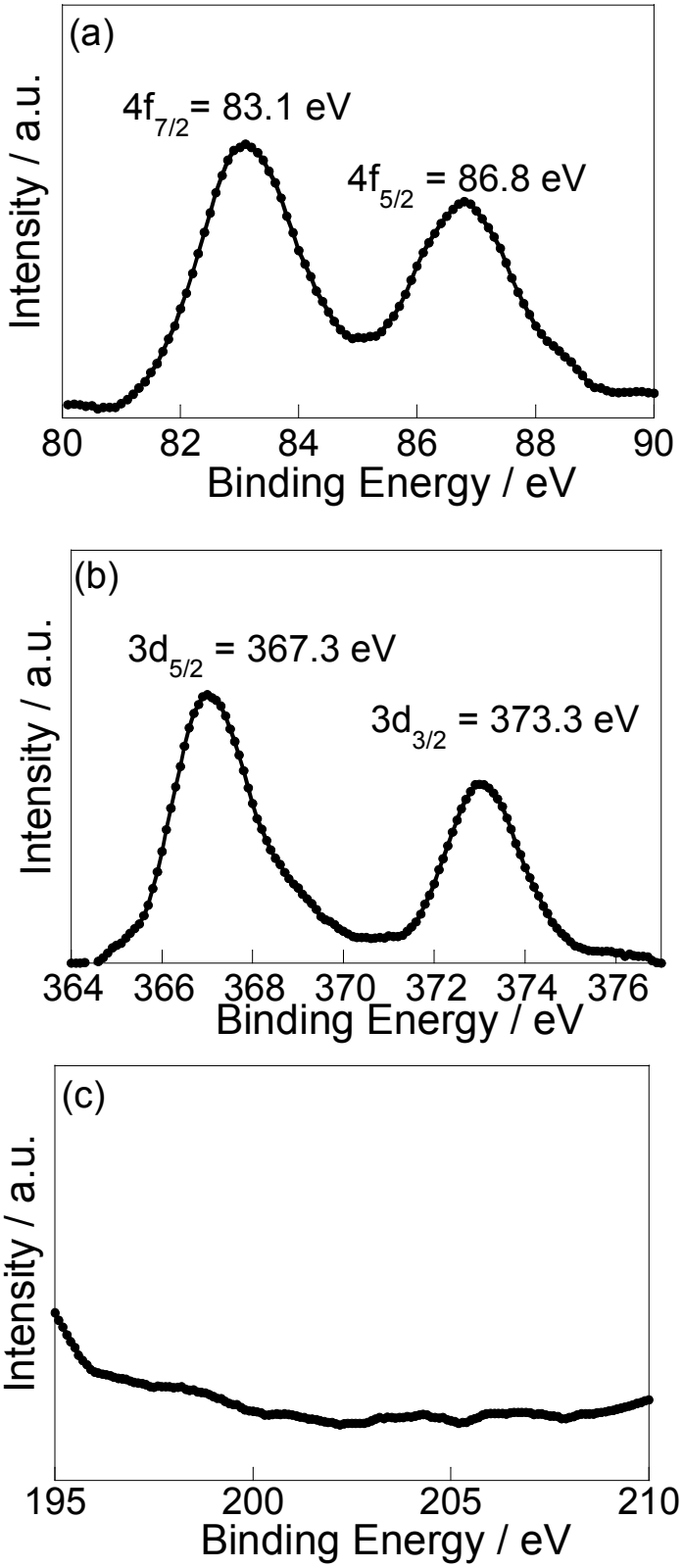

Figure 2.4 XPS spectra for Au 4f doublets (a) and Ag 3d doublets (b) of the AuAg alloy nanoparticles and Cl 2S(c).

2.4 Conclusions

The size of Ag nanoparticles prepared by sputter deposition of Ag onto BMI-PF_6 and their concentration varied depending on sputtering conditions, such as magnitude of discharge current. Sputtered Ag species caused reduction of $HAuCl_4$ in the IL, resulting in the formation of AuAg alloy nanoparticles. The chemical composition and optical property of the alloy nanoparticles were easily controlled by changing the concentration of HAuCl4, though the size distribution was slightly broadened in comparison with the method of using Au and Ag binary metal target. Although only AuAg alloy was prepared in the present study, various metal and alloy nanoparticles can be prepared in IL by appropriately selecting the metal to be sputter-deposited on ILs to reduce different metal ions. Furthermore, since highly reactive metals, such as Zn and Li, are in principle vacuum- deposited onto ILs to form nanoparticles, this technique will be useful for the development of novel chemical reactions in ILs under vacuum using ultrafine metal nanoparticles as reagents.

2.5 References

(1) Jana, N. R.; Gearheart, L.; Murphy, C. *J., Chem. Mater.* **2001,** 13, 2313.

(2) Murray, C. B.; Norris, D. J.; Bawendi, M. G., *J. Am. Chem. Soc.* **1993,** 115, 8706.

(3) Sawai, Y.; Takimoto, B.; Nabika, H.; Ajito, K.; Murakoshi, K., *Faraday Discuss.* **2006,** 132, 179.

(4) Schmid, G., *Chem. Rev.* **1992,** 92, 1709.

(5) Templeton, A. C.; Wuelfing, M. P.; Murray, R. W., *Acc. Chem. Res.***2000,** 33, 27.

(6) Cole, A. C.; Jensen, J. L.; Ntai, I.; Tran, K. L. T.; Weaver, K. J.; Forbes, D. C.; Davis, J. H., *J. Am. Chem. Soc*. **2002,** 124, 5962.

(7) Gu, Y. L.; Ogawa, C.; Kobayashi, J.; Mori, Y.; Kobayashi, S., *Angew. Chem. Int. Edit.* **2006,** 45, 7217.

(8) Gelesky, M. A.; Umpierre, A. P.; Machado, G.; Correia, R. R. B.; Magno, W. C.; Morais, J.; Ebeling, G.; Dupont, J., *J. Am. Chem. Soc*. **2005,** 127, 4588.

(9) Wang, Y.; Yang, H., *Chem. Commun.* **2006**, 2545.

(10) Quinn, B. M.; Ding, Z. F.; Moulton, R.; Bard, A. J., *Langmuir* **2002,** 18, 1734.

(11) Endres, F.; Bukowski, M.; Hempelmann, R.; Natter, H., *Angew. Chem. Int. Edit.* **2003,** 42, 3428.

(12) Scheeren, C. W.; Machado, G.; Teixeira, S. R.; Morais, J.; Domingos, J. B.; Dupont, J., *J. Phys. Chem. B* **2006,** 110, 13011.

(13) Fonseca, G. S.; Umpierre, A. P.; Fichtner, P. F. P.; Teixeira, S. R.; Dupont, *J. Dupont, Chem. Eur. J.* **2003,** 9, 3263.

(14) Itoh, H.; Naka, K.; Chujo, Y., *J. Am. Chem. Soc*. **2004,** 126, 3026.

(15) Torimoto, T.; Okazaki, K.; Kiyama, T.; Hirahara, K.; Tanaka, N.; Kuwabata, S., *Appl. Phys. Lett.* **2006,** 89, 243117.

(16) Okazaki, K. I.; Kiyama, T.; Hirahara, K.; Tanaka, N.; Kuwabata, S.; Torimoto, T., *Chem. Commun.* **2008**, 691.

(17) Okazaki, K.; Kiyama, T.; Suzuki, T.; Kuwabata, S.; Torimoto, T., *Chem. Lett.* **2009**, 38, 330.

(18) Tsuda, T.; Kurihara, T.; Hoshino, Y.; Kiyama, T.; Okazaki, K.; Torimoto, T.; Kuwabata, S., *Electrochemistry* **2009**, 77, 693.

(19) Kameyama, T.; Ohno, Y.; Kurimoto, T.; Okazaki, K.; Uematsu, T.; Kuwabata, S.; Torimoto, T., *Phys. Chem. Chem. Phy.* **2010**, 12, 1804.

(20) Tsuda, T.; Yoshii, K.; Torimoto, T.; Kuwabata, S., *J. Power Sources* **2010**, 195, 5980.

(21) Oda, Y.; Hirano, K.; Yoshii, K.; Kuwabata, S.; Torimoto, T.; Miura M. *Chem. Lett.* **2010**, 39, 1069.

(22) Khatri, O. P.; Adachi, K.; Murase, K.; Okazaki, K.; Torimoto, T.; Tanaka, N.; Kuwabata, S.; Sugimura, H., *Langmuir* **2008**, 24, 7785.

(23) Torimoto, T.; Tsuda, T.; Okazaki, K.; Kuwabata, S., *Adv. Mater*. **2010**, 22, 1196.

(24) Kuwabata, S.; Tsuda, T.; Torimoto, T., *J. Phys. Chem. Lett.* **2010**, 1, 3177.

(25) Meiss, S. A.; Rohnke, M.; Kienle, L.; El Abedin, S. Z.; Endres, F.; Janek, J., *Chemphyschem* **2007,** 8, 50.

(26) El Abedin, S. Z.; Polleth, M.; Meiss, S. A.; Janek, J.; Endres, F., *Green Chem.* **2007,** 9, 549.

(27) Imanishi, A.; Tamura, M.; Kuwabata, S., *Chem. Commun.* **2009**, 1775.

(28) Hatakeyama, Y.; Okamoto, M.; Torimoto, T.; Kuwabata, S.; Nishikawa, K.,. *J. Phys. Chem.C* **2009**, 113, 3917.

(29) Hatakeyama, Y.; Takahashi, S.; Nishikawa, K., *J. Phys. Chem.C* **2010**, 114, 11098.

(30) Wender, H.; de Oliveira, L. F.; Migowski, P.; Feil, A. F.; Lissner, E.; Prechtl, M. H. G.; Teixeira, S. R.; Dupont, J., *J. Phys. Chem.C* **2010**, 114, 11764.

(31) Sun, Y. G.; Wiley, B.; Li, Z. Y.; Xia, Y. N., *J. Am. Chem. Soc*. **2004,** 126, 9399.

(32) Lu, X. M.; Tuan, H. Y.; Chen, J. Y.; Li, Z. Y.; Korgel, B. A.; Xia, Y. N., *J. Am. Chem. Soc*. **2007,** 129, 1733.

(33) Link, S.; Wang, Z. L.; El-Sayed, M. A., *J. Phys. Chem. B* **1999,** 103, 3529.

(34) Watson, R. E.; Hudis, J.; Perlman, M. L., *Phys. Rev. B* **1971,** 4, 4139.

Chapter 3

Synthesis of Transition Metal Oxide Nanoparticles Highly Dispersed in Ionic Liquids by Sputter Deposition Technique

3.1 Introduction

Nanoparticles are well known materials to enhance and/or to change the original characters of bulk.[1-5] Transition metal oxide nanoparticles are particular importance for various fields of science and technology, such as in the field of heterogeneous catalysis,[6] where they are used as catalyst supports for a wide variety of metals or as selective oxidation catalysts by themselves. Applications to electric devices and sensors are also important because metal oxides can be used as insulators, semiconductors, conductors, and even superconductors. These characters result from the electronic states in the bulk or localized surface states. Hence, there is much interest in how the character changes with change in the size of metal oxide nanoparticles. There are several proposed methods for fabricating metal oxide nanoparticles, and they can be classified into physical and chemical techniques: physical methods include sputtering (dc, RF and reactive), evaporation (thermal and electron beam) [7] and pulse laser deposition, [8] and chemical methods include sol-gel, co-precipitation,

impregnation, chemical vapor synthesis and hydrothermal treatment[9-12]. Ionic liquid (IL) are suitable media for the synthesis of metal oxide nanoparticles by decomposition of metal carbonyl or alkoxide,[13,14] because ILs are utilized as non-flammable, non-volatile solvents. Metal and alloy nanoparticles were prepared with a sputter-deposition of metal onto ILs and a chemical reaction in solution, as described in Chapter 2. This fact suggests that various kinds of chemical reactions can be induced, depending on the redox potential of metal nanoparticles. For instance, if highly reactive metal, such as Ti, of relatively more negative oxidation potentials are sputter deposited in ILs, the metal species can be acted as a precursor to form metal oxide nanoparticles, because they are easy oxidized by air and/or moisture. However, such as synthesis in the form of nanometer-sized particles attempt has not been made yet. Therefore, oxide nanoparticles can be easily prepared.

In this chapter, we applied the method to synthesis of metal oxide nanoparticles in ILs by sputter deposition of transition metals of tungsten (W), molybdenum (Mo), niobium (Nb), and titanium (Ti) onto IL, and corresponding metal oxide nanoparticles of less than 6 nm in size were produced.

3.2 Experimental Section

3.2.1 Materials

1-ethyl-3-methylimidazolium tetrafluoroborate (EMI-BF_4) was purchased from Kanto Chemical. Octadecane-1-thiol was purchased from Tokyo Chemical Industry. Other chemicals used in this study were supplied from Kishida Reagents Chemicals

3.2.2 Synthesis of metal oxide nanopaeticles by sputter deposition onto ionic liquids

I used a DC sputtering apparatus (Sanyu Electron Co., Ltd, SC-701HMCII) with four metal targets of W, Mo, Nb, and Ti. The IL (EMI-BF_4) was dried for 3 h at 393 K under vacuum just before use. A 0.60 cm^3 portion of the dried IL solution was spread on a glass plate (10 cm^2) which was horizontally set in the DC sputtering apparatus. The glass plate was 2.0 cm away from the metal target. After pre-sputtering for 10 min to clean the metal target, metal sputter-deposition into EMI-BF_4 was carried out for 20 min under 2.0 Pa of Ar gas (>99.9999%) with 40 mA of ion current.

3.2.3 Characterization of nanoparticles.

The size distribution and shape of nanoparticles formed in EMI-BF_4 were determined by TEM (HITACHI H-7650) operated at an acceleration voltage of 100 kV. TEM samples were prepared by dipping a copper TEM grid with amorphous carbon overlayers (Oken shoji, #10-1012) into the thus-obtained EMI-BF_4. The excess amount of IL was rinsed off with acetonitrile, followed by drying under a vacuum condition. Additionally, elemental compositions and crystallographic structures of nanoparticles were analyzed by XPS (JEOL JPS-9000MC) and XRD (RIGAKU 2100HL), respectively. For the preparation of XPS and XRD samples, the nanoparticles in the thus-obtained IL were precipitated by a 5 mmol dm^{-3} octadecane-1-thiol/ethanol solution, followed by centrifugation. The concentrated nanoparticles were settled on a small Si substrate.

3.3 Results and Discussion

Figure 3.1 shows typical TEM images of nanoparticles synthesized by sputter deposition of W, Mo, Nb and Ti targets in EMI-BF_4. Strong and vague contrasts were observed; the former was assigned to nanoparticles obtained by sputter deposition, and the latter could be attributed to the residue of EMI-BF_4 after washing with acetonitrile. The nanoparticles were well dispersed, and no secondary particle formation was observed.

Figure 3.2 shows the size distribution of nanoparticles obtained by measurements of the diameter of 100 nanoparticles in TEM images. Most of the nanoparticles were spherical or polyhedral in shape, and no anisotropic type was found. The ranges of particle size were 3.2~4.8 nm for W target, 2.7~3.7 nm for Mo target, 1.9~2.9 nm for Nb target, and 3.4~4.6 nm for Ti target. Average diameters (D_{ave}) of nanoparticles obtained for Mo and Nb sputtering were 3.2 and 2.4 nm, respectively, being relatively smaller than those for W and Ti targets (D_{ave} = 4.0 in both cases). The size distributions of nanoparticles prepared from the Mo or Nb targets were quite narrow, in which the standard deviations (σ) were 0.5 nm.

Figure 3.3 shows XPS spectra of the obtained nanoparticles. The solid lines indicate observed data after subtracting background variation of photoelectron spectra. The dotted lines and the dashed line indicate peak separation results and a summation of the

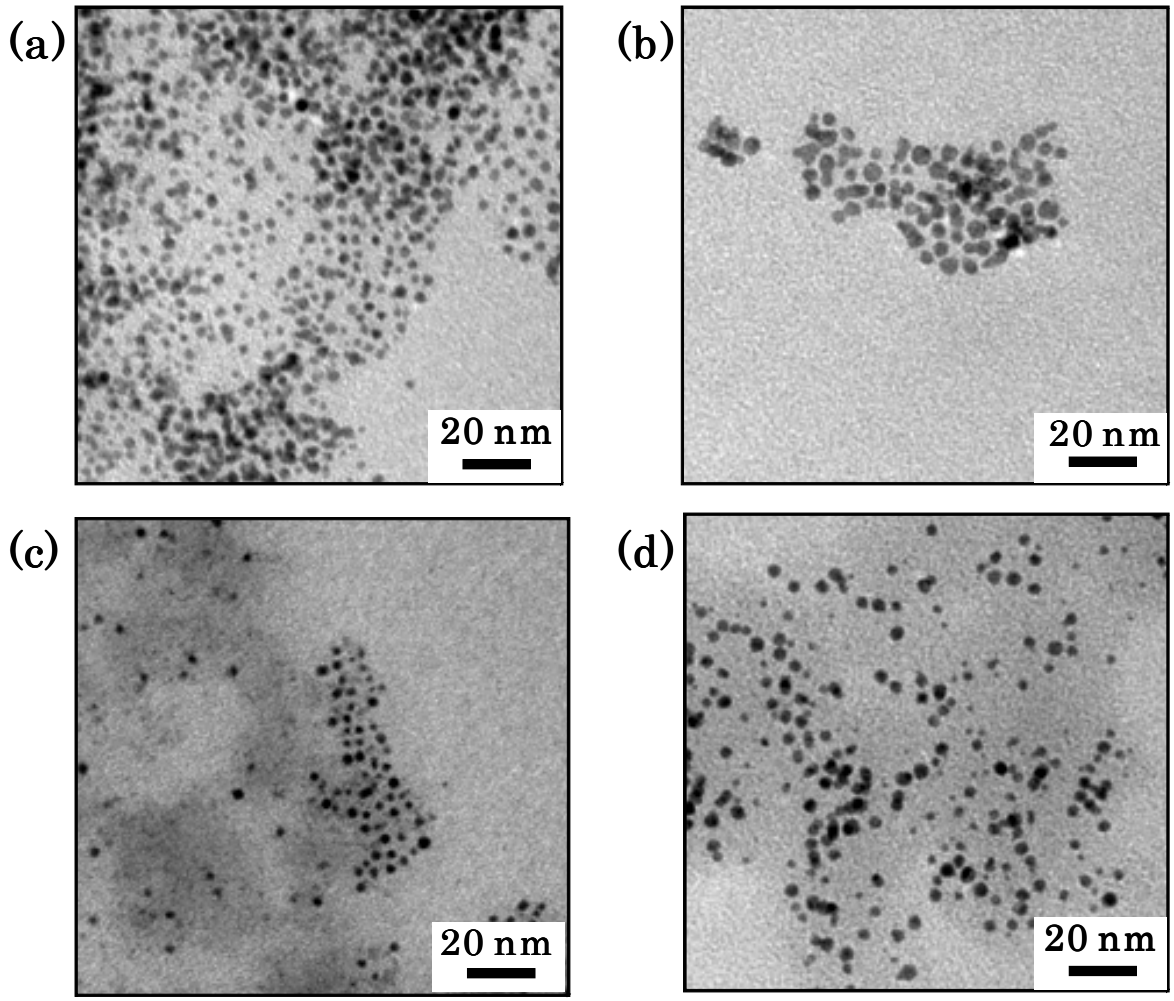

Figure 3.1 Typical TEM images of nanoparticles obtained by sputter deposition of transition metal targets: (a) W, (b) Mo, (c) Nb and (d) Ti into ionic liquids of EMI-BF_4

results, respectively. In all cases, I observed not only a metal phase but also oxide phases. From the XPS peak analysis, at least two oxide phases could be recognized and the total amount of oxide phases was more than 80% in all cases. Further XPS analysis showed that fluorine and sulfur were involved in each case. Typical representatives are shown in Figure 3.3(a) and (b), respectively. The former was attributed to the residue of the IL of EMI-BF_4,

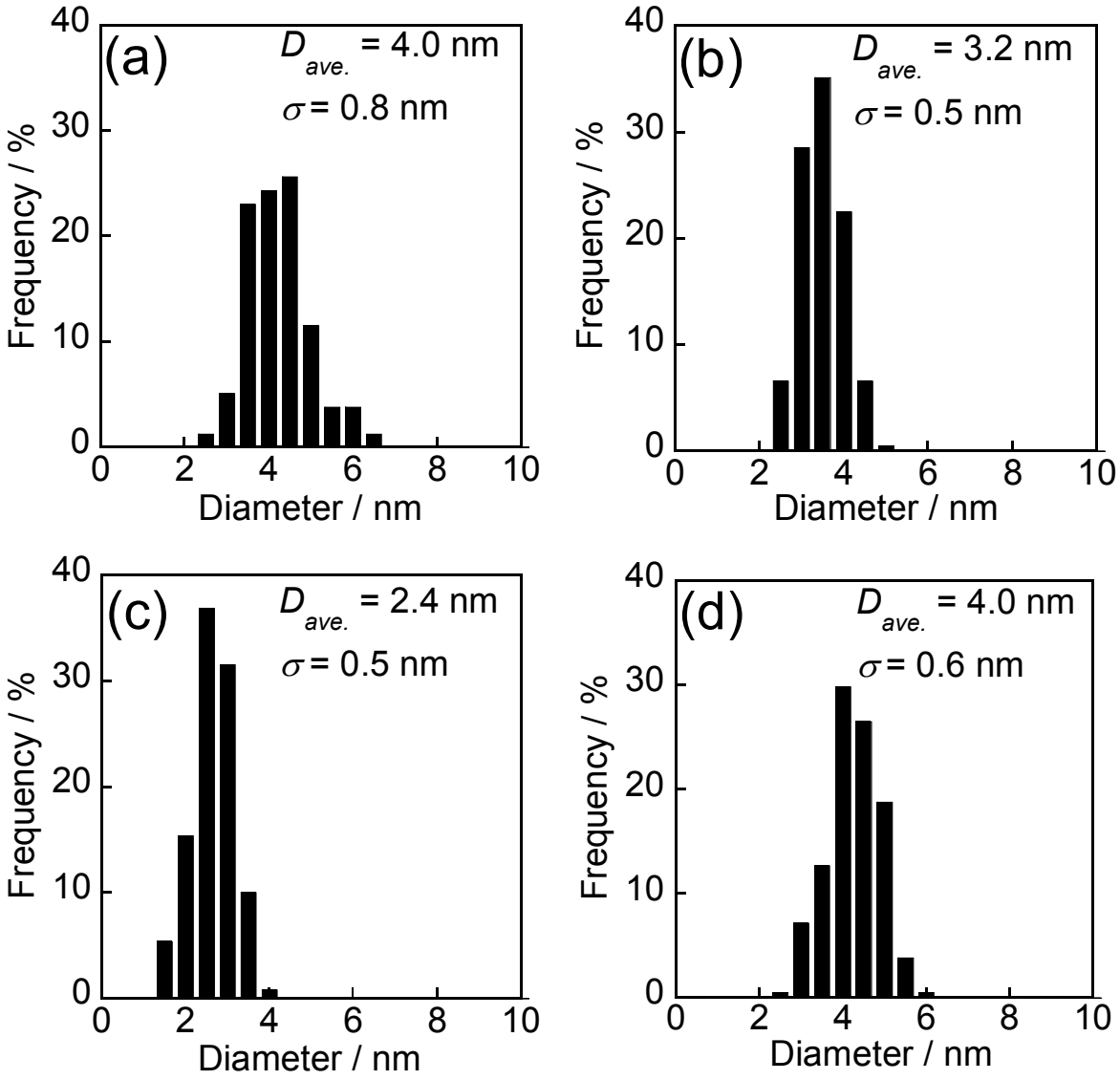

Figure 3.2 Size distributions of nanoparticles obtained by sputter deposition of (a) W, (b) Mo, (c) Nb and (d) Ti targets into ionic liquids of EMI-BF_4, derived from Figure 3.1.

and the latter originated from the octadecane-1-thiol used in the preparation of XPS samples. These species were difficult to remove completely by repeating the washing procedures, indicating that these species were strongly adsorbed on the nanoparticle surfaces.

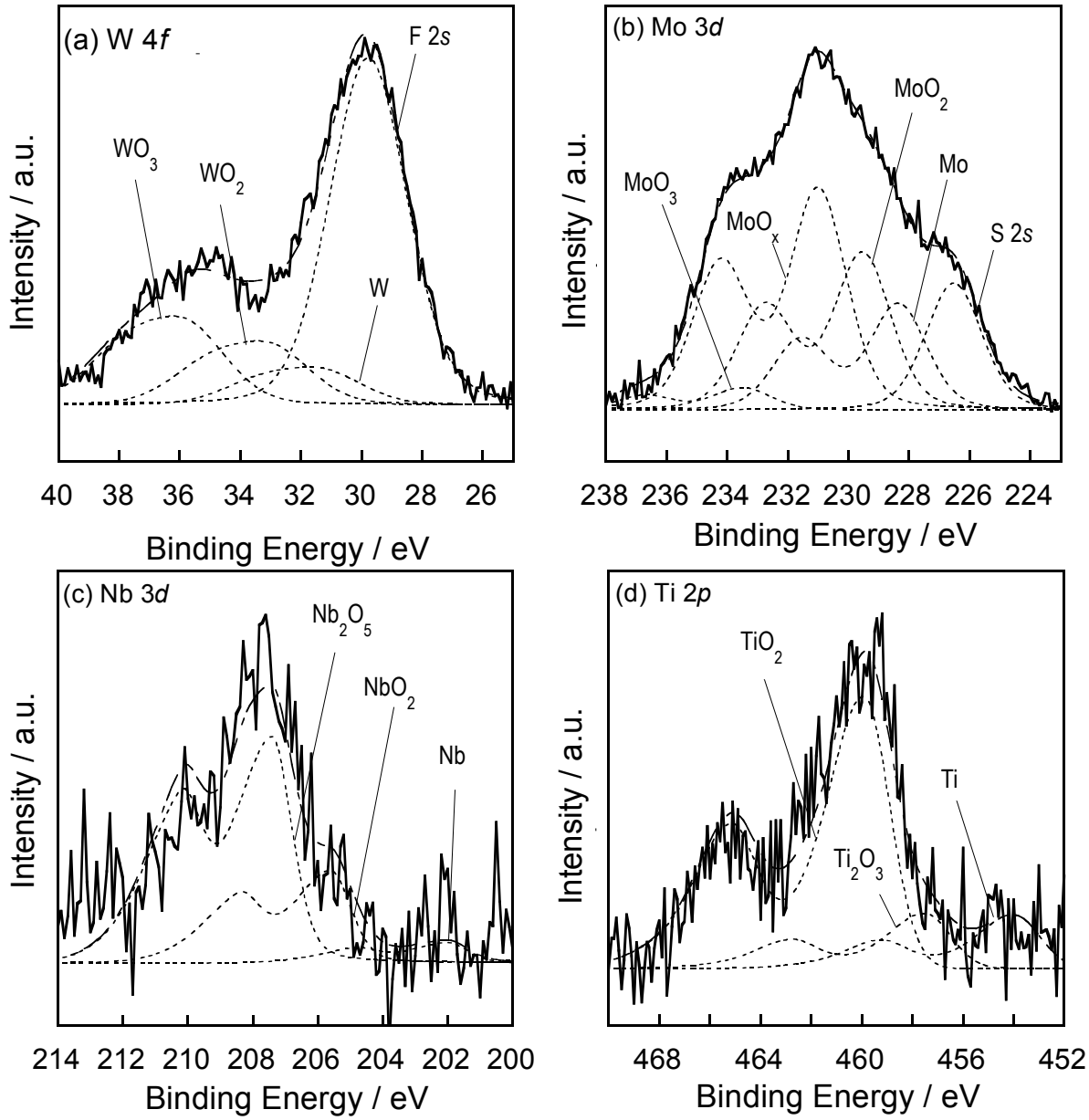

Figure 3.3 XPS spectra for nanoparticles obtained by sputter deposition of (a) W, (b) Mo, (c) Nb and (d) Ti targets into ionic liquids of EMI-BF_4.

Figure 3.4 shows XRD pattern of the obtained nanoparticles. As can be seen from the figure, the peak of origin at lattice intervals of these metals were observed at around 40º. The crystallite size of thus-obtained these metals were estimated from the full width at half

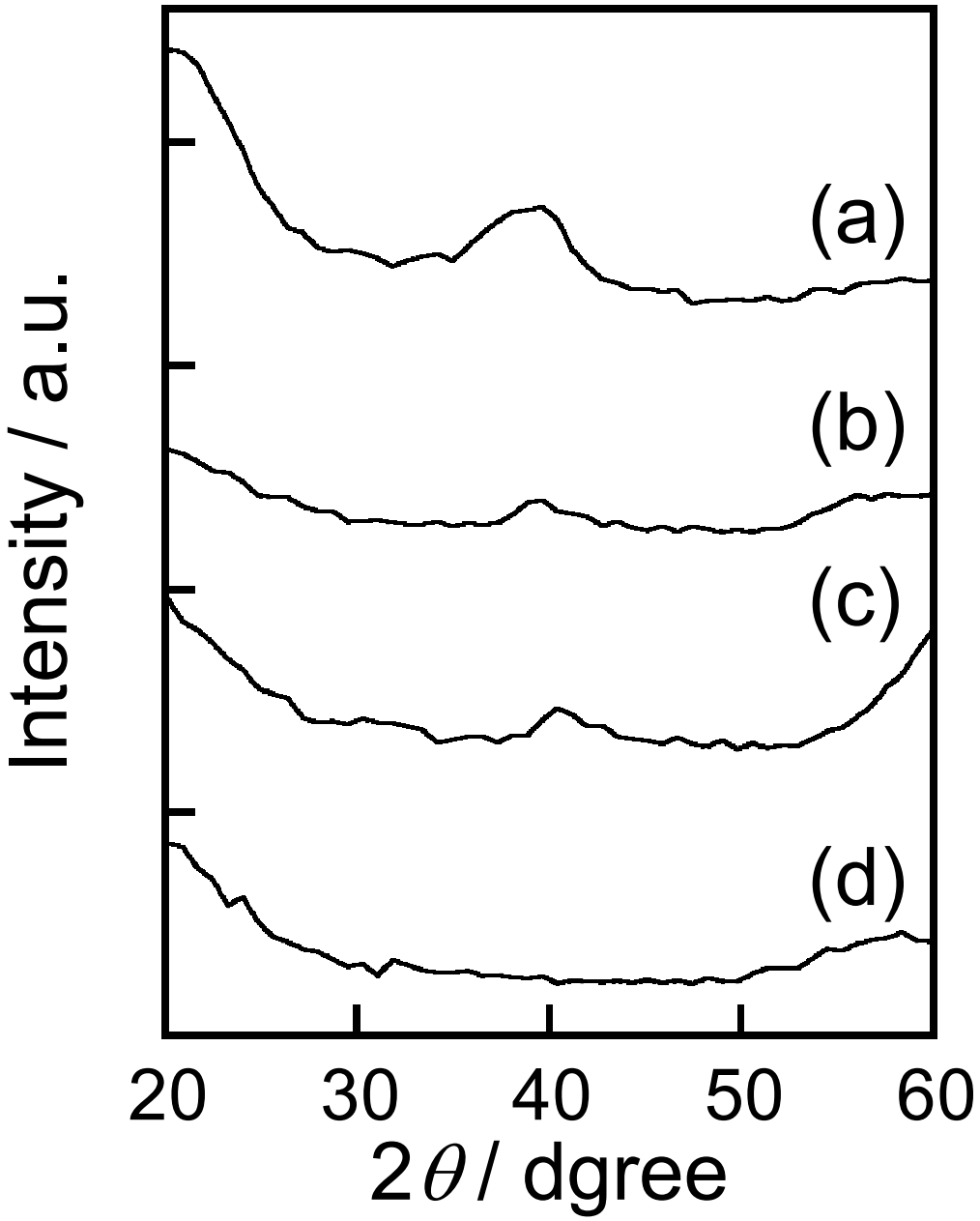

Figure 3.4 XRD patterns for nanoparticles obtained by sputter deposition of (a) Nb, (b) W, (c) Ti and (d) Mo targets into ionic liquids of EMI-BF_4.

maximum of main peak by using the Scherrer equation. The crystallite size of W, Nb and Ti were 3.1, 1.8 and 2.4 nm, respectively. The size of Mo could not be measured, because the crystallite size was small. The estimated values decreased at about 20-40% from the

nanoparticle size obtained from TEM. I expected that the change was due to oxidation of the metal nanoparticle. From the result of XPS spectrum, about 80% of the obtained nanoparticle was the oxide, although no peak corresponding to crystal phases of these oxides was found in the XRD measurements. The amorphous oxide phases were probably formed by oxidization of metal nanoparticles in the IL.

Torimoto et al. previous studies on Au, Ag and Pt nanoparticles, they concluded that the IL could stabilize the metal nanoparticles without aggregation of Nanoparticles[15-25]. The local structure of the IL surrounding the nanoparticle might have a role to protect the nanoparticles from uncertain transformation. Actually, I did not find any oxidized nanoparticles in these experiments. In the present study, however, I observed that the metals of W, Mo, Nb, and Ti sputter-deposited in IL were oxidized to form metal oxide nanoparticles. This means that the IL layer of EMI-BF_4 on the nanoparticle surface did not have an ability enough to protect the oxidation of nanoparticles of the transition metal having negative oxidation potentials from oxidants contained in the IL as impurities. Nevertheless, the metal phases still remained in each XPS spectrum, suggesting that oxidization reaction of metal nanoparticles was limited by initial concentrations of oxidants or did not rapidly proceed in the IL. I propose oxygen and/or water molecules as possible candidates of oxidants. Before the sputter deposition, we actually dried the IL for 3 h at 393 K under vacuum in the

order of 10^{-1} Pa, but the degree of vacuum might not have been sufficient to completely remove the dissolved water introduced from the atmosphere in advance. Alternatively, the metal nanoparticles might have been oxidized by oxygen molecules that were contained as an impurity in Ar gas and/or dissolved into the IL from air during sample preparation for TEM, XPS, and XRD. Such dissolved oxidants may affect the stability of metal nanoparticles in IL and oxidize metal nanoparticles to form amorphous oxide phases. Although it is difficult to synthesize metal oxide nanoparticles having various diameters with a single oxidation state of metal atoms at the present, I expect further precise control of the concentration of oxidants and /or temperature of IL during the sputter deposition provides both the uniform composition of nanoparticles and the tenability in the nanoparticle size.

3.4 Conclusions

I have synthesized transition metal oxide nanoparticles of WO_x, MoO_x, NbO_x and TiO_x by sputter deposition in the IL of EMI-BF_4. These metal oxide nanoparticles were obtained in a dispersed manner with the size of 3.2~4.8 nm for W, 2.7~3.7 nm for Mo, 1.9~2.9 nm for Nb, 3.4~4.6 nm for Ti. These results indicate that sputter deposition in IL has the potential to provide various types of highly dispersed transition metal oxide

nanoparticles without any additional stabilizing agent to prevent aggregation of nanoparticles.

3.5 References

(1) Takimoto, B.; Nabika, H.; Murakoshi, K., *J. Phys. Chem. C* **2009**, 113, 11751.

(2) Imanishi, A.; Tamura, M.; Kuwabata, S., *Chem. Commun.* **2009**, 1775.

(3) Nosaka, Y.; Shibamoto, M.; Nishino, J., *J. Colloid. Interf. Sci.* **2002**, 251, 230.

(4) Saruyama, M.; Kanehara, M.; Teranishi, T., *J. Am. Chem. Soc.* **2010**, 132, 3280.

(5) Yamada, S., *Anal. Sci.* **2009**, 25, 1059.

(6) Moshfegh, A. Z., *J. Phys. D Appl. Phys.* **2009**, 42, 233001.

(7) Martirosyan, K. S.; Luss, D., *Chem. Eng. Technol*. **2009**, 32, 1376.

(8) Liu, Z.; Yuan, Y.; Khan, S.; Abdolvand, A.; Whitehead, D.; Schmidt, M.; Li, L., *J. Micromech. Microeng*. **2009**, 19, 054008.

(9) Bilecka, I.; Djerdj, I.; Niederberger, M., *Chem. Commun*. **2008**, 886.

(10) Makela, J. M.; Keskinen, H.; Forsblom, T.; Keskinen, J., *J. Mater. Sci.* **2004**, 39, 2783.

(11) Bumajdad, A.; Eastoe, J.; Zaki, M. I.; Heenan, R. K.; Pasupulety, L., *J. Colloid. Interf. Sci.* **2007**, 312, 68.

(12) Chen, L.; Xu, J.; Tanner, D. A.; Phelan, R.; Van der Meulen, M.; Holmes, J. D.; Morris,

M. A., *Chem.-Eur. J.* **2009**, 15, 440.

(13) Redel, E.; Thomann, R.; Janiak, C., *Chem. Commun*. **2008**, 1789.

(14) Kramer, J.; Redel, E.; Thomann, R.; Janiak, C., *Organometallics* **2008**, 27, 1976.

(15) Torimoto, T.; Tsuda, T.; Okazaki, K.; Kuwabata, S., *Adv. Mater*. **2010**, 22, 1196.

(16) Torimoto, T.; Okazaki, K.; Kiyama, T.; Hirahara, K.; Tanaka, N.; Kuwabata, S., *Appl. Phys. Lett.* **2006**, 89, 243117.

(17) Okazaki, K. I.; Kiyama, T.; Hirahara, K.; Tanaka, N.; Kuwabata, S.; Torimoto, T., *Chem. Commun* .**2008**, 691.

(18) Suzuki, T.; Okazaki, K.; Kiyama, T.; Kuwabata, S.; Torimoto, T., *Electrochemistry* **2009**, 77, 636.

(19) Okazaki, K.; Kiyama, T.; Suzuki, T.; Kuwabata, S.; Torimoto, T., *Chem. Lett.* **2009**, 38, 330.

(20) Tsuda, T.; Kurihara, T.; Hoshino, Y.; Kiyama, T.; Okazaki, K.; Torimoto, T.; Kuwabata, S., *Electrochemistry* **2009**, 77, 693.

(21) Kameyama, T.; Ohno, Y.; Kurimoto, T.; Okazaki, K.; Uematsu, T.; Kuwabata, S.; Torimoto, T., *Phys. Chem. Chem. Phy.* **2010**, 12, 1804.

(22) Khatri, O. P.; Adachi, K.; Murase, K.; Okazaki, K.; Torimoto, T.; Tanaka, N.; Kuwabata, S.; Sugimura, H., *Langmuir* **2008**, 24, 7785.

(23) Oda, Y.; Hirano, K.; Yoshii, K.; Kuwabata, S.; Torimoto, T.; Miura M. *Chem. Lett.* **2010**, 39, 1069.

(24) Tsuda, T.; Yoshii, K.; Torimoto, T.; Kuwabata, S., *J. Power Sources* **2010**, 195, 5980.

(25) Kuwabata, S.; Tsuda, T.; Torimoto, T., *J. Phys. Chem. Lett.* **2010**, 1, 3177.

Chapter 4

Synthesis of Indium Metal Nanoparticles and Hollow Indium Oxide Nanoparticles via the Sputter Deposition Technique in Ionic Liquids

4.1 Introduction

Structure control of metal and semiconductor nanoparticles in nanometer scale has attracted much attention because physicochemical properties, such as optical properties and catalytic activities, can be varied depending on the size and shape of nanoparticles.[1-6] Recently, ionic liquids (ILs) have been considered to be excellent media for the formation and stabilization of nanoparticles.[7-9] Noble metal nanoparticles were prepared in ILs without addition of stabilizing agents or capping molecules, in contrast to the synthesis in aqueous or conventional organic solvents, which inevitably requires the addition of stabilizing agents. For example, stable noble metal nanoparticles, such as Ir, Rh and Au, were chemically synthesized in ILs by chemical reduction of the corresponding metal ions or thermal decomposition of organometallic compounds.[10-12] Although many strategies for the preparation of noble metal nanoparticles have been reported, highly reactive metal

nanoparticles, such as Zn and In, which have relatively more negative redox potentials, have been difficult to synthesize in the form of nanometer-sized particles because of the instability of nanoparticles induced by easy oxidation reaction in air.

Recently, the extremely low vapor pressure of ILs has enabled researchers to treat them under vacuum conditions. Endres et al. reported synthesis of Ag nanoparticles in an IL by reduction of Ag ions in the IL with electrons produced by a glow discharge (plasma-electrochemical deposition) under reduced pressure conditions.[15,16] Torimoto et al. reported a very clean method for synthesizing noble nanoparticles, such as Au, Ag, and Pt, in ILs using a sputter deposition technique without any additives.[17-27] The size of prepared nanoparticles varied depending on the kind of IL used.[17]

Furthermore, as demonstrated in Chapter 2 and 3, alloy and oxide nanoparticles were prepared with a sputter-deposition of metal onto ILs and using redox reactions. The sputter deposition of highly reaction metal nanoparticles produced composite nanoparticles composed of metal and metal oxide as shown in Chapter 3, though the detained structures of the nanoparticles were not known.

Nanoparticles of indium (In) metal have attracted much attention because they are expected to act as nanometer-sized lubricants or novel catalysts for organic syntheses. Nanoparticles of In have been useful as a starting material for the preparation of

nanostructured In-based materials because indium is a highly reactive metal and the reaction of nanosized In metal with chemical species containing elements of V or VI groups can produce semiconductor nanoparticles such as InP, InAs, and In_2O_3.[28-30] In nanoparticles have been prepared by several synthetic strategies, such as reduction of In^{3+} ions with strong reducing agents,[31] thermal decomposition of organometallic precursors,[32] laser ablation,[33] metal vapor deposition,[34] and dispersion of molten In into paraffin oil.[35] On the other hand, the preparation of nano-structured In_2O_3 is also attractive because their applications are expected in wide research areas, such as gas sensors,[36] solar cells,[37] flat-panel displays,[38] and photocatalysts.[39] One of the attractive strategies for preparation of In_2O_3 nanoparticles has been oxidation of In nanoparticles.[40] The shape of the resulting In_2O_3 nanoparticles is expected to be reflected by that of the starting In metal nanoparticles, but the details are not reported for nanometer-sized particles.

In this chapter, I prepared In metal nanoparticles in ILs by the sputter deposition technique. The thus-obtained In nanoparticles were used as a starting material to fabricate nanostructured In_2O_3 particles, and heat treatment of ILs containing In metal nanoparticles in air enabled the formation of hollow In_2O_3 nanoparticles highly dispersed in IL.

4.2 Experimental Section

4.2.1 Materials

N,N,N,-trimethyl-N-propylammonium bis(trifluoromethylsulfonyl)amide (TMPA-TFSA), 1-butyl-3-methylimidazolium bis(trifluoromethylsulfonyl)amide (BMI-TFSA), 1-ethyl-3-methylimidazolium tetrafluoroborate (EMI-BF_4), 1-butyl-3-methylimidazolium tetrafluoroborate (BMI-BF_4), 1-allyl -3-methylimidazolium tetrafluoroborate (AMI-BF_4) and 1-allyl-3-ethylimidazolium tetrafluoroborate (AEI-BF_4) were purchased from Kanto Chemical. 1-hexyl-3-methylimidazolium tetrafluoroborate (HMI-BF_4), 1-octyl-3-methylimidazolium tetrafluoroborate (OMI-BF_4) and 1-butyl-2,3-dimethylimidazolium tetrafluoroborate (BMMI-BF_4) were purchased from Merck. Other chemicals used in this study were supplied from Kishida Reagents Chemicals.

4.2.2 Synthesis of indium nanoparticles by sputter deposition onto ionic liquids.

Sputter deposition of indium in ILs was performed using a sputter coater (Sanyu Electron Co., Ltd, SC-701HMCII) with a sputtering current of 10 mA under argon (> 99.99%) pressure of 2.0 Pa at room temperature. An IL (0.60 cm^3) was spread on a glass plate (10 cm^2) that was horizontally set in the sputter coater. The surface of the IL was located at a distance of 20 mm from the indium foil target (99.99% in purity). The sputtering was carried out for 10 min. After the sputter deposition of In, the vacuum chamber was filled with air and then IL solution was collected from the glass plate.

4.2.3 Heat treatment of indium nanoparticles in air.

In the case of oxidation of In nanoparticles, a 0.10 cm^3 portion of thus-obtained IL solution was put in a test tube, followed by heat treatment in air at various temperatures for 1 hour without agitation.

4.2.4 Characterization of nanoparticles.

The size and shape of nanoparticles formed in ILs were observed using a transmission electron microscope (TEM; HITACHI H-7650) operated at an acceleration voltage of 100 kV. High-resolution transmission electron micrographs of nanoparticles were

obtained using a JEOL 2010F TEM operated at 200 kV. Samples for TEM measurements were prepared by dropping an IL solution containing nanoparticles onto a copper grid with amorphous carbon overlayers (Oken Shoji, #10-1012), and then the excess amount of IL was washed out by dropping a small amount of acetonitrile, followed by drying under vacuum. The size distribution of nanoparticles in ILs was also obtained by dynamic light scattering operated at 298 K using an Otuka Electronics FDLS-3000.

The crystal structure of nanoparticles was investigated by an X-ray powder diffraction (XRD) analysis using a RIGAKU 2100HL with Cu Kα radiation. X-ray photoelectron spectroscopy (XPS) measurements were performed using a JEOL JPS-9000MC with irradiation of Al Kα. Samples for XRD measurements were prepared by isolation of nanoparticles with the addition of a large amount of methanol to the IL solutions. The precipitates were collected by centrifugation, followed by washing with methanol several times and drying under vacuum.

4.3 Results and discussion

4.3.1 Characterization of nanoparticles synthesized by In sputter deposition onto EMI-BF_4.

The XRD pattern of the product obtained sputter deposition of indium in EMI-BF_4 is shown in Figure 4.1. As can be seen from the figure, several peaks were observed and they were assigned to the body-centered tetragonal (bct) crystal structure of In metal.[41] No perceivable peaks assigned to its derivatives, such as In_2O_3, were observed.[42] The crystallite size of thus-obtained In metal was estimated to be 4.8 nm from the full width at half maximum of the (101) peak by using the Scherrer equation.[43] In contrast, observation of the dynamic light scattering (DLS) showed that the as-deposited nanoparticles in ILs had a wide size distribution ranging from 7 to 10 nm (Figure 4.2), and the average diameter was determined to 8.1 nm. This value was remarkably different from the crystallite size estimated from XRD. These facts suggested that the surface of In metal nanoparticles was covered with an amorphous layer as supported by the following TEM measurements.

Figure 4.3a shows a typical TEM image of the nanoparticles obtained by In sputter deposition in EMI-BF_4. Spherical nanoparticles were observed without the formation of aggregated secondary particles. It was clearly recognized that individual nanoparticles had

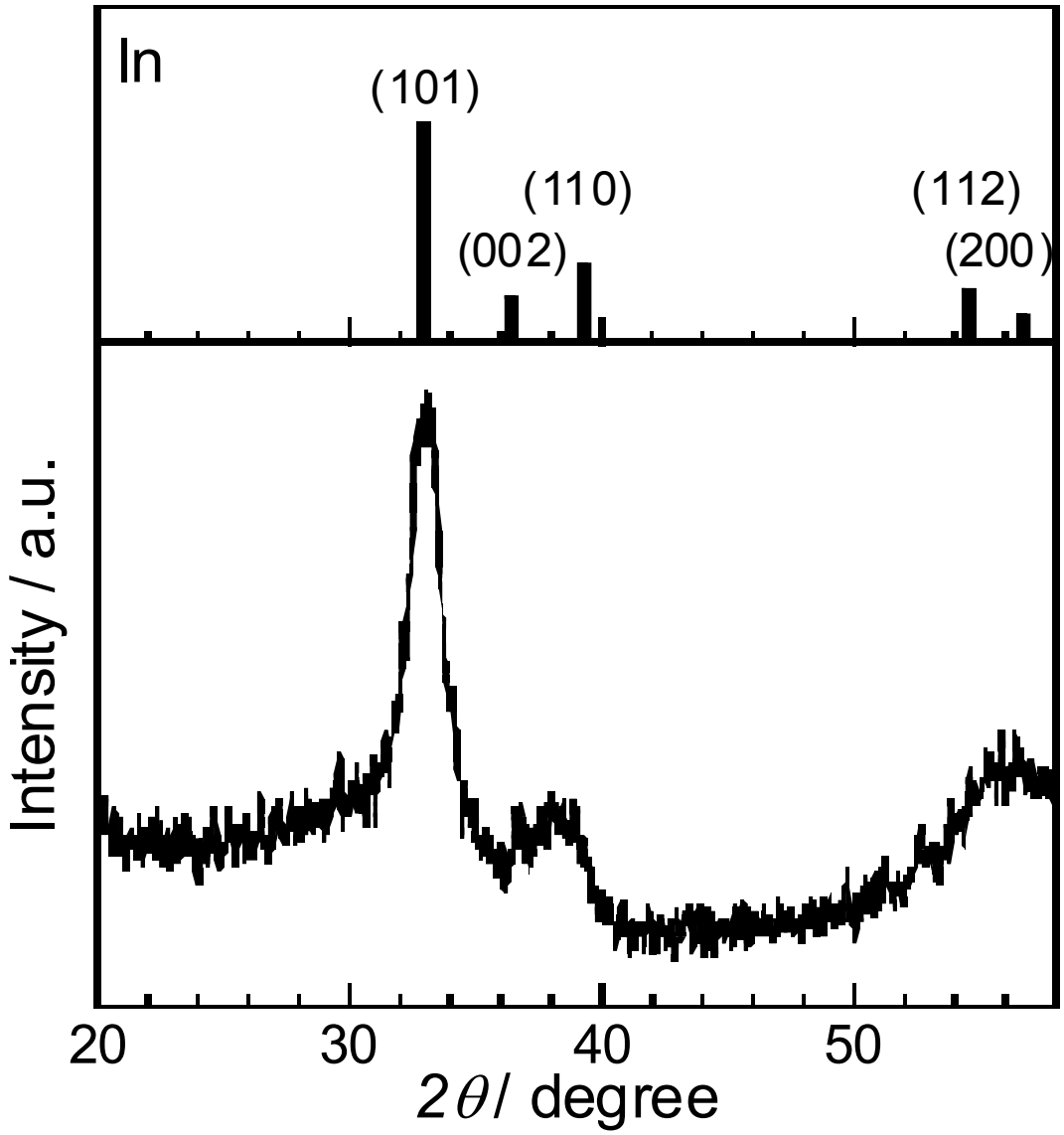

Figure 4.1 An XRD pattern of nanoparticles prepared by In sputter deposition in EMI-BF_4.

a core/shell structure, with the core showing a darker image than the surface shell layer. Furthermore, even when the sample stage of the TEM was tilted at angles from -30 to +30º, a similar core/shell structure was seen in TEM images for each nanoparticles (Figure 4.4); that is, the dark image was located at the center of the nanoparticles, indicating that the core was

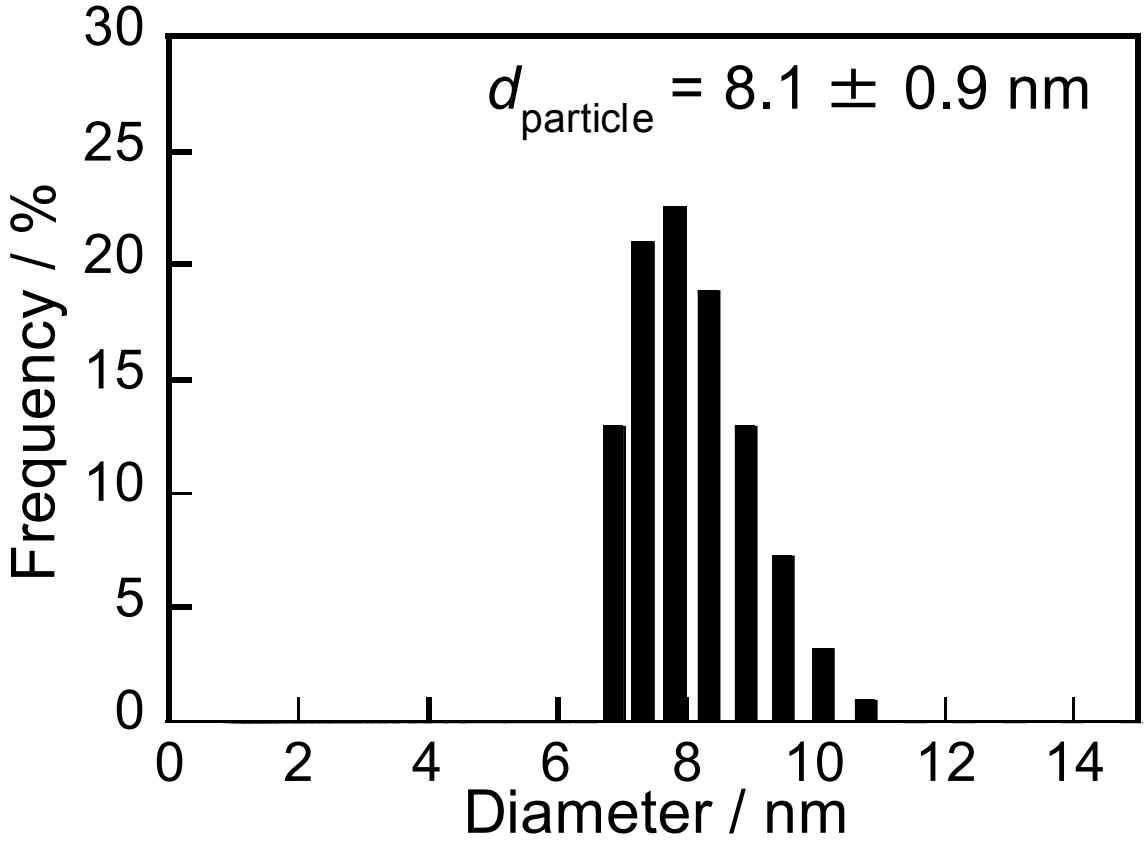

Figure 4.2 Size distribution of as-sputter-deposited particles in EMI-BF_4 obtained by DLS measurement.

located almost at the center of the particle and then the shell having a uniform thickness covered the core surface. Figure 4.3b shows an HRTEM image of the core/shell nanoparticles. The core of darker image in a particle exhibited clear lattice fringes without exhibiting lattice mismatch or lattice defects inside the core. The interplanar spacing of lattice fringes was calculated to be 0.27 nm, which was assigned to the (101) plane of indium metal,[41] indicating that the core was a single crystal made of In metal and was covered with

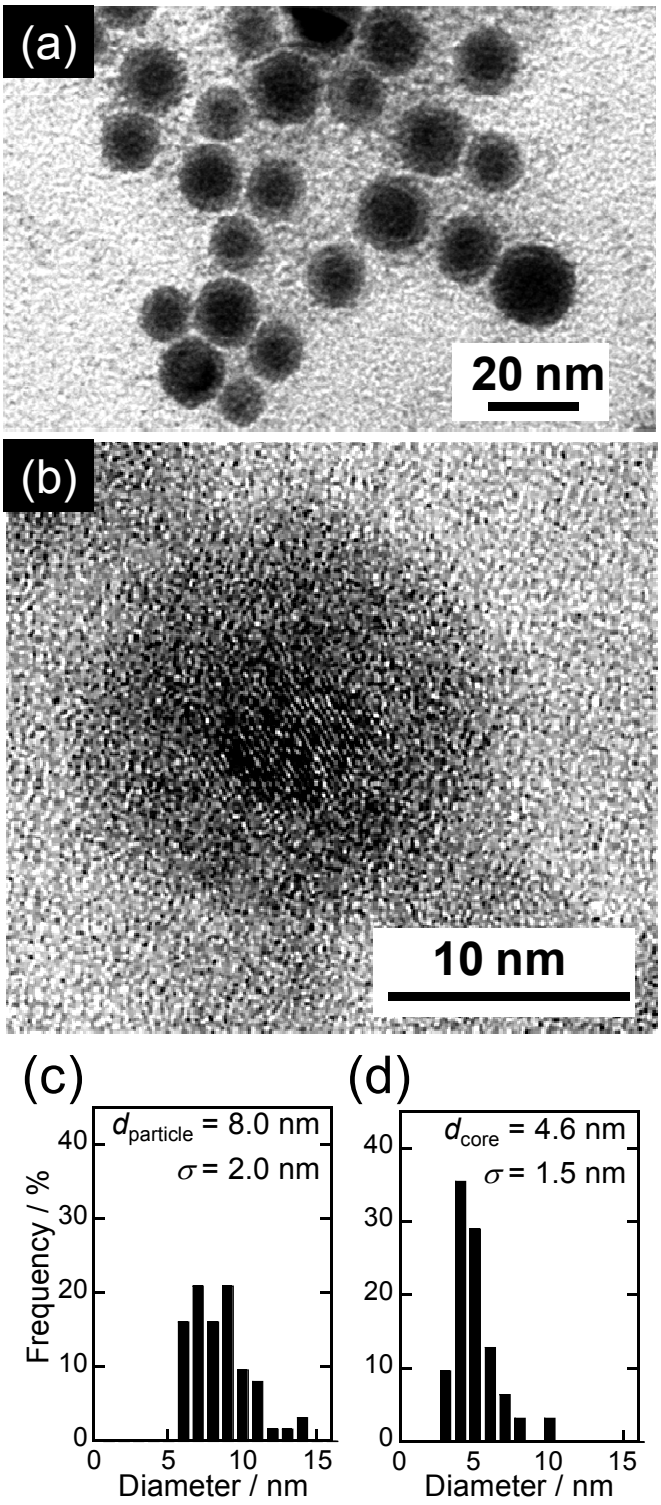

Figure 4.3 (a) A typical TEM image of nanoparticles prepared by In sputter deposition in EMI-BF_4. (b) A high magnification image of a nanoparticle in figure (a). (c) Size distribution of whole particles having an In/In_2O_3 core/shell structure and (d) that of In cores inside the particles obtained from TEM images.

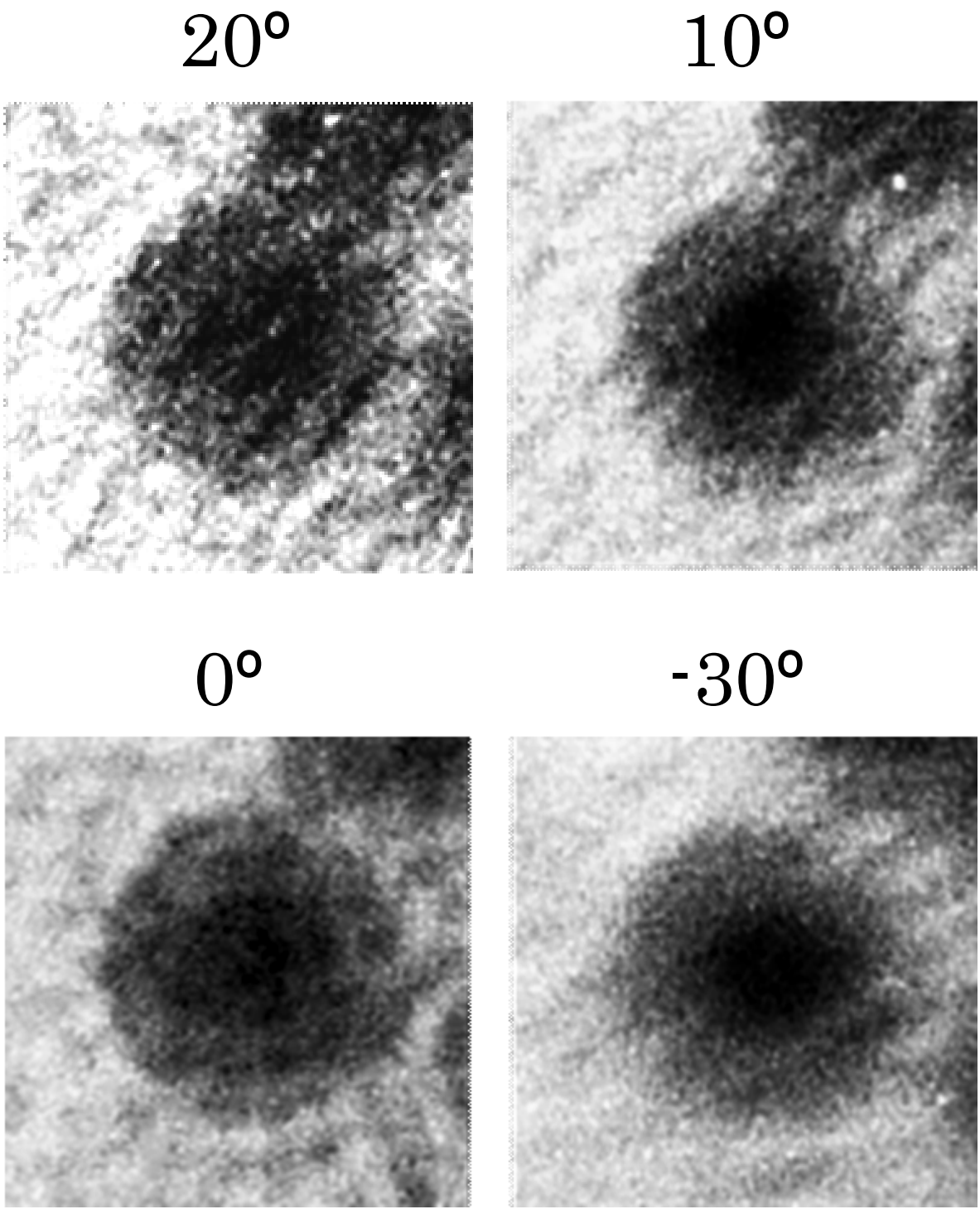

Figure 4.4 Typical TEM images of core/shell nanoparticles prepared by the In sputter deposition in EMI-BF_4. Images were taken at various tilt angles of the sample holder from 20º to -30º.

an amorphous shell layer.

Figure 4.5 shows XPS spectra of the core/shell nanoparticles shown in Figure 4.3a in the range of binding energies corresponding to the signals of In 3d and O 1s. Signals assigned to In $3d_{5/2}$ and In $3d_{3/2}$ were observed at 444.8 and 452.5 eV, respectively.[45] These peaks were shifted toward higher energy from the binding energies of the indium metal (In^0) but agreed with those of In_2O_3. In addition, the peaks originating from O 1s were composed of two spectral bands at 533.5 and 531.6 eV. The signal at 531.6 eV could be attributed to the lattice oxygen in In_2O_3 and that at 533.5 eV was assignable to H_2O probably adsorbed on the nanoparticles surface.[46,47] Since XPS spectra were sensitive for the surface of the nanoparticles, these results indicated that the nanoparticles as-sputter-deposited had a surface composed of indium (III) oxide. Consequently, based on the results of XRD, XPS and TEM observations, I could concluded that In sputter deposition in EMI-BF_4 produced core/shell-structured nanoparticles composed of a single-crystalline In metal core and amorphous In_2O_3 shell layer. The size distribution of nanoparticles was determined by TEM measurements as shown in Figure 4.3a (more than 100 particles). Figure 4.3c and 4.3d show the size distribution of whole nanoparticles having a core/shell structure and that of In cores in the nanoparticles. The average size of the whole nanoparticles ($d_{particle}$) was determined to be 8.0 nm with standard deviation (σ) of 2.0 nm, which was comparable to the size

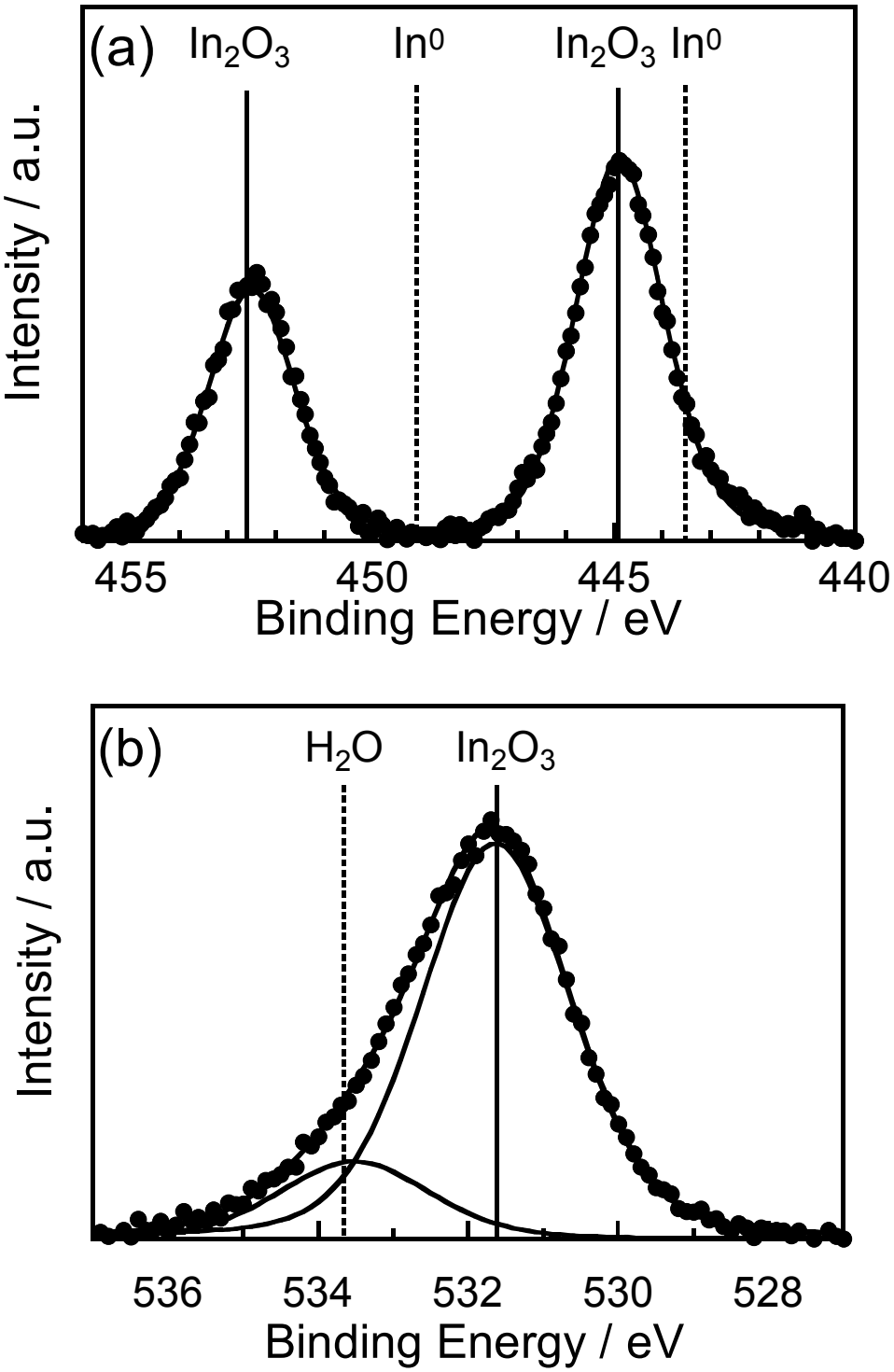

Figure 4.5 XPS spectra for In 3d doublets (a) and O 1s (b) of the core/shell nanoparticles.

determined by DLS measurement (8.1 nm), indicating that nanoparticles were highly dispersed in ILs without large aggregation. The cores of In metal had an average size (d_{core}) of 4.6 nm (σ of 1.5 nm), which was in good agreement with the size estimated from the XRD peak (4.8 nm). The shell thickness could be estimated to be 1.7 nm assuming that it was half the difference between $d_{particle}$ and d_{core}.

The expected mechanism for the formation of In/In_2O_3 core/shell nanoparticles is partial oxidation of In metal nanoparticles with O_2 contained in argon gas as an impurity or in air. Bombardment of the In foil surface with energetic argon ions caused physical ejection of surface atoms or small clusters, which were injected in IL. This situation could make a high concentration of In species on the surface of IL to coalesce with each other, resulting in the production of nanometer-sized In particles. Since In metal has a sufficient redox potential to be oxidized with O_2 and the surface energy of nanoparticles is generally high, the surface of In nanoparticles was rapidly oxidized to form an In_2O_3 shell layer by exposure of the IL solution to air after the sputter deposition. The density of the In_2O_3 shell seems to be sufficient to prevent further oxidation of the In metal core, resulting in the formation of stable In/In_2O_3 core/shell nanoparticles.

4.3.2 Synthesis of In_2O_3 hollow structure nanoparticles via heat treatment in air.

The thus-obtained EMI-BF_4 solution containing In/In_2O_3 core/shell nanoparticles was heated at various temperatures for 60 min in air. Figure 4.6 shows the changes in extinction spectra of the In-deposited EMI-BF_4 solution with increase in heat treatment temperature. An absorption shoulder appeared at 280 nm for In/In_2O_3 core/shell nanoparticles, which was assigned to the surface plasmon resonance (SPR) peak of In nanoparticles.[34,36,48] The intensity of the peak at 280 nm was diminished with an increase in temperature and then completely disappeared with heat treatment at 523 K, indicating that degradation of the In metal core occurred with heat treatment. This was supported by the results of XRD analyses.

Figure 4.7 shows XRD patterns of the nanoparticles heat-treated at various temperatures. The crystal phase of In metal was detected for samples treated at temperatures below 373 K, but the intensity of the XRD peaks was lessened with an increase in heating temperature, the behavior being accordance with the results observed in the extinction spectra. Heat treatment at temperatures higher than 423 K caused disappearance of the peaks originating from the In metal. From TEM image, although as-sputter-deposited core/shell nanoparticles completely disappeared, spherical nanoparticles of uniformly contrast were formed (Figure 4.8). Whereas broad diffraction peaks assigned to the (222) lattice planes of

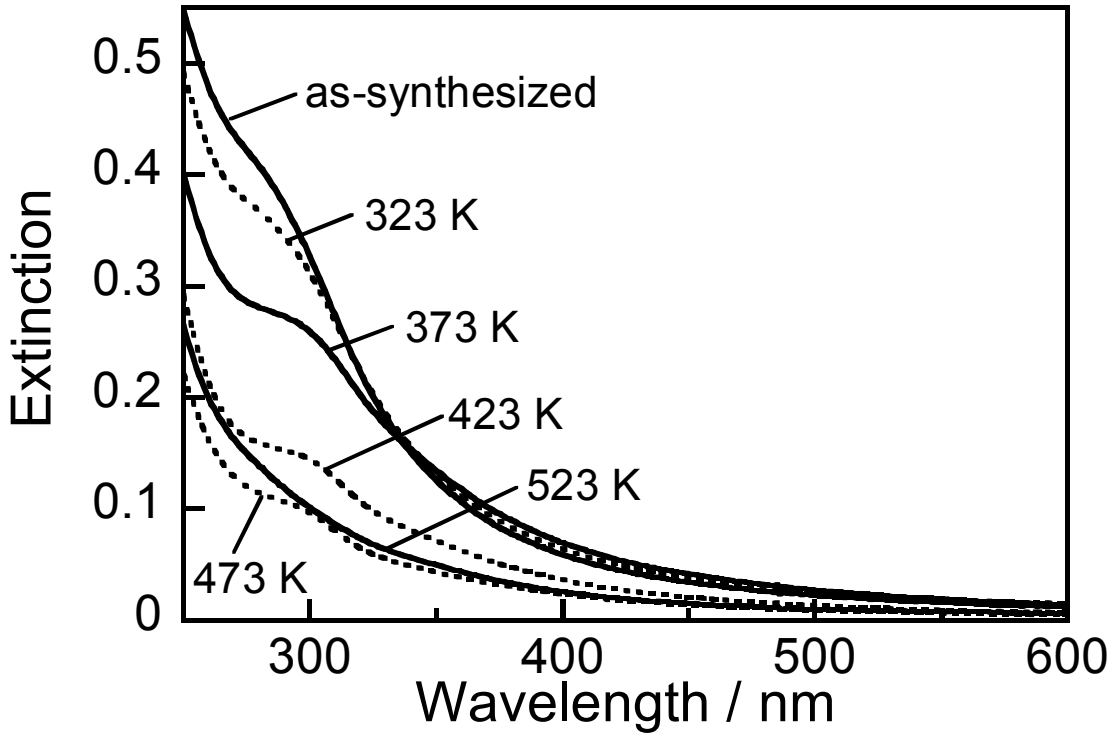

Figure 4.6 Changes in extinction spectra of In-sputter-deposited EMI-BF_4 solution with heat treatment in air at various temperatures. The temperatures are indicated in the figure.

In_2O_3 emerged at around $2\theta = 30^o$ by heat treatment at 473 K and then a highly crystallized In_2O_3 phase was produced at 523 K.[42] Considering that the melting point of In is 419 K,[49] these facts suggested that the In metal cores melted with heating at temperature higher than 423 K and then were easily oxidized with O_2 to form In_2O_3.

Figure 4.9a shows a TEM image of crystalline In_2O_3 nanoparticles obtained with heat treatment at 523 K. Although as-sputter-deposited core/shell nanoparticles completely disappeared, spherical nanoparticles with a hollow interior were formed. TEM images of the

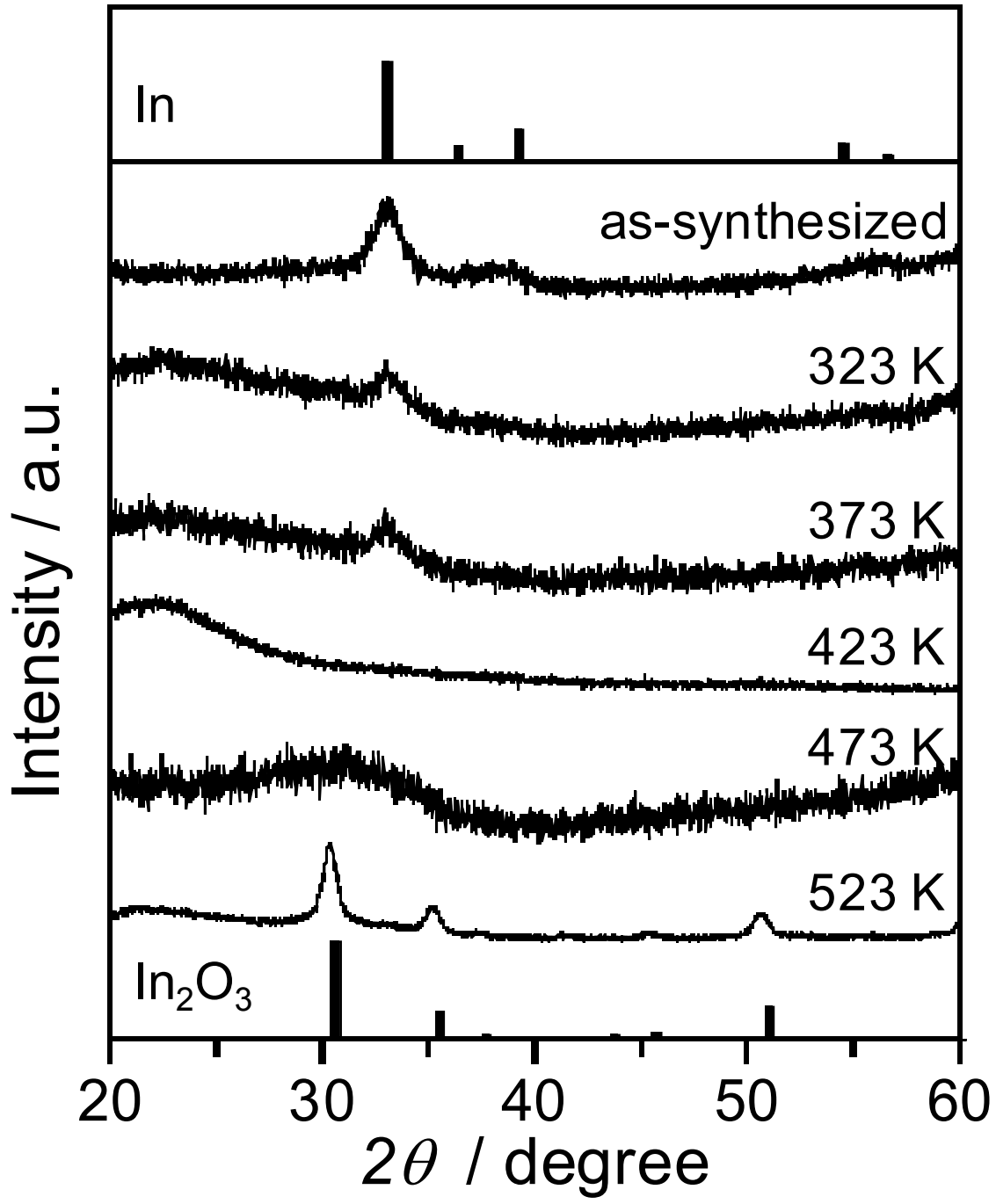

Figure 4.7 XRD patterns of the nanoparticles shown in Fig.4.6. The temperatures are indicated in the figure.

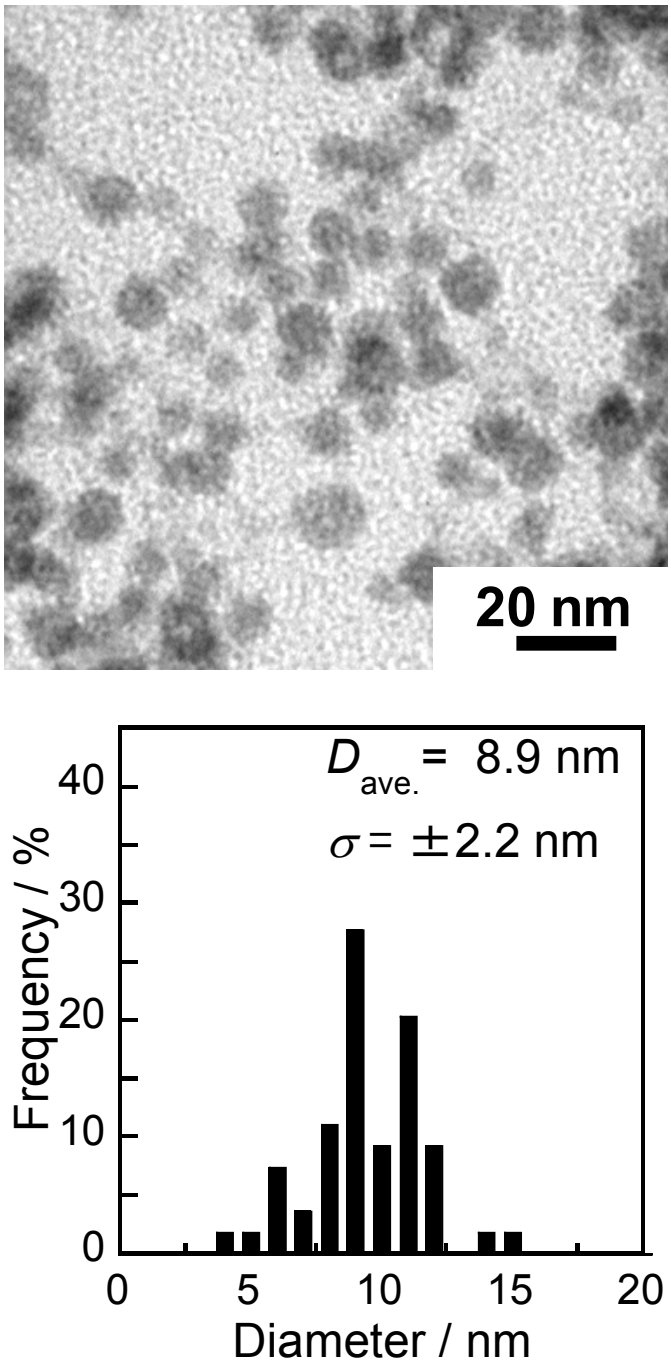

Figure 4.8 TEM images of Indium nanoparticles obtained after heat treatment at 423 K in air.

individual nanoparticles were almost unchanged when the measurements were performed by changing the tilt angle of the TEM sample holder (Figure 4.10). This fact indicated that the spherical hollow In_2O_3 nanoparticles were formed by heat treatment with the void space being located at almost the center of each particle. An HRTEM image (Figure 4.9b) revealed that hollow nanoparticles had a polycrystalline shell wall composed of nanoparticles having clear lattice fringes with an interplanar spacing of 0.29 nm corresponding to the (222) of cubic In_2O_3 phase.

Figure 4.9c and 4.9d show the size distributions of hollow nanoparticles and their void spaces determined by TEM measurements. Hollow nanoparticles had a wide size distribution ranging from 6 to 13 nm, and the average diameter of whole nanoparticles ($d_{particle}$) was determined to 8.1 nm (σ of 1.5 nm), which was slightly larger than that of the In/In_2O_3 core/shell nanoparticles used as a starting material, $d_{particle}$ of 8.0 nm. In contrast, a void space smaller than the size of the In core was formed; void spaces in hollow nanoparticles with an average size (d_{void}) of 4.1 nm (σ of 0.9 nm) were formed by heating the core/shell nanoparticles with In core size of 4.6 nm. By halving the difference between $d_{particle}$ and d_{void} of hollow nanoparticles, the shell thickness could be estimated to 2.0 nm, being slightly thicker than that of the shell thickness of original core/shell nanoparticles.

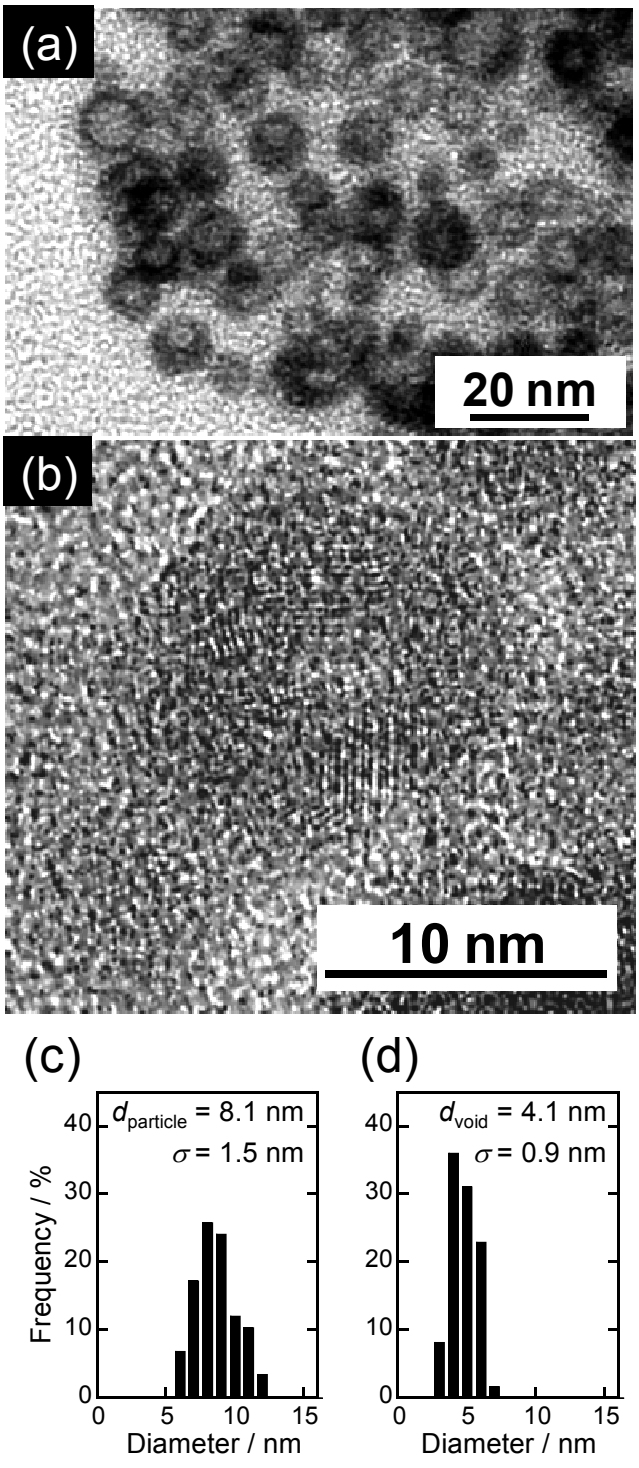

Figure 4.9 (a) A typical TEM image of nanoparticles in EMI-BF_4 obtained after heat treatment at 523 K in air. (b) A high magnification image of a hollow nanoparticle in figure (a). (c) Size distribution of In_2O_3 hollow nanoparticles and (d) that of their void spaces obtained from TEM images.

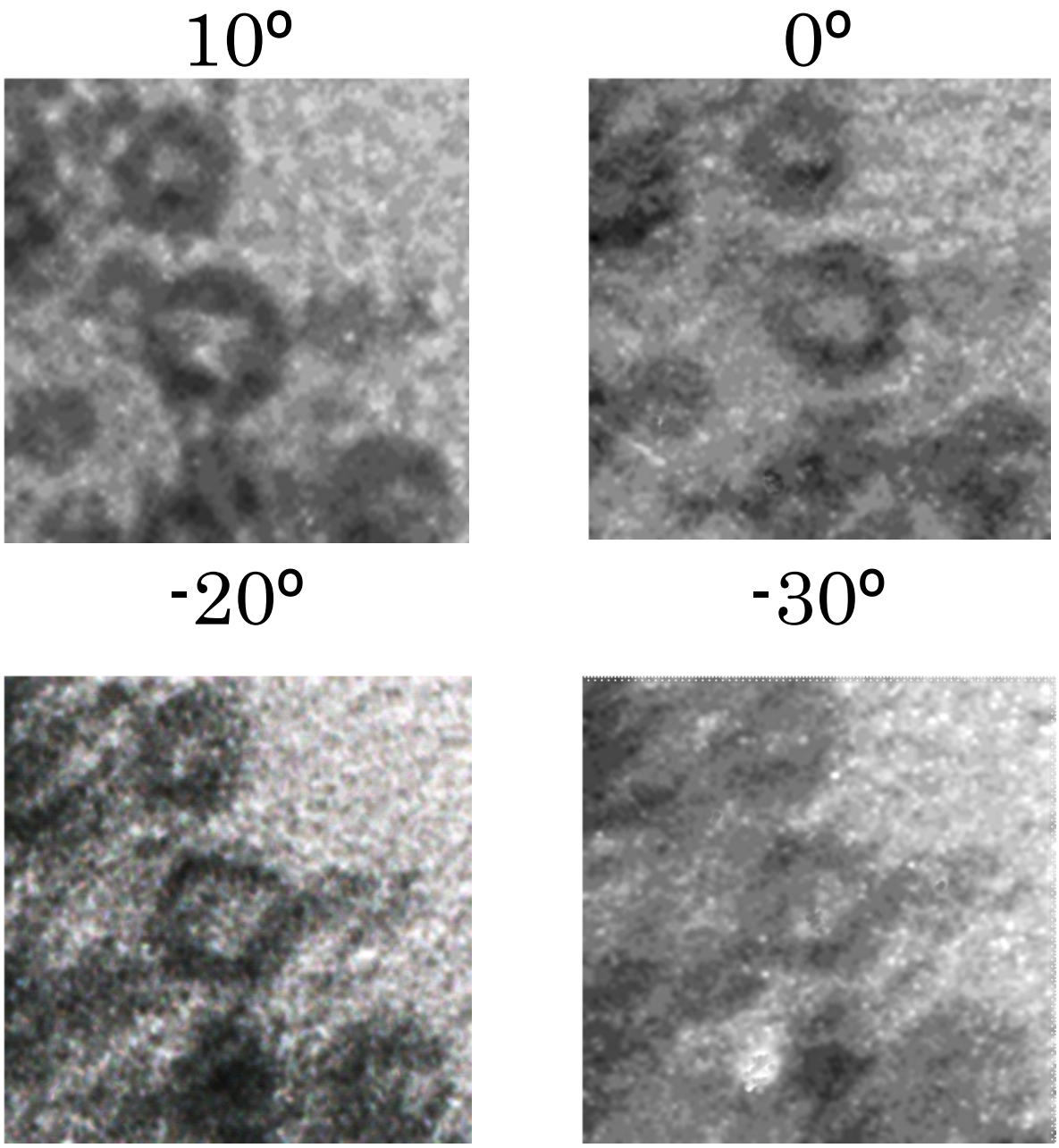

Figure 4.10 Typical TEM images of hollow nanoparticles prepared by heat treatment at 523 K. Images were taken at various tilt angles of the sample holder from 10º to -30º.

4.3.3 Size control of the In/In_2O_3 core/shell structure nanoparticles and the resulting In_2O_3 hollow structure nanoparticles.

The size control of In nanoparticles was examined by the similar method in Chapter 2. TEM images of In nanoparticles prepared under different sputter conditions are shown in Figure 4.11. Spherical nanoparticles with the core/shell structure were observed in all cases, although the particle size did not changed apparently. In Chapter 2, the size of Ag nanoparticles increased up-to 1.4 nm larger than the initial size with increasing the sputtering current from 10 to 20 mA, while the size of In nanoparticles was not the case. At the present, there is not clean explanation on the difference between them. The phenomenon might be related to formation of core/shell structure in the case of In nanoparticles, which means that oxidation process probably reduced the size of In nanoparticles.

On the other hand, it has been reported that the size of nanoparticles formed in ILs varied depending on the kind of ILs used.[17,50,52] Therefore, I tried to control the size of In nanoparticles by changing the kind of IL. Figure 4.12 and 4.13 shows TEM images of particles obtained by In sputter deposition in the different type of BF_4-base and TFSA-based ILs. Sputter deposition of In could be produced nanoparticles in all cases. Average diameters were 5.6 nm for BMMI-BF_4, 7.4 nm for HMI-BF_4, 5.7 nm for OMI-BF_4 (Figure 4.12) and 9.7 nm for BMI-BF_4, 16.8 nm for AEI-BF_4, 18.2 nm for AMI-BF_4, (Figure 4.13).

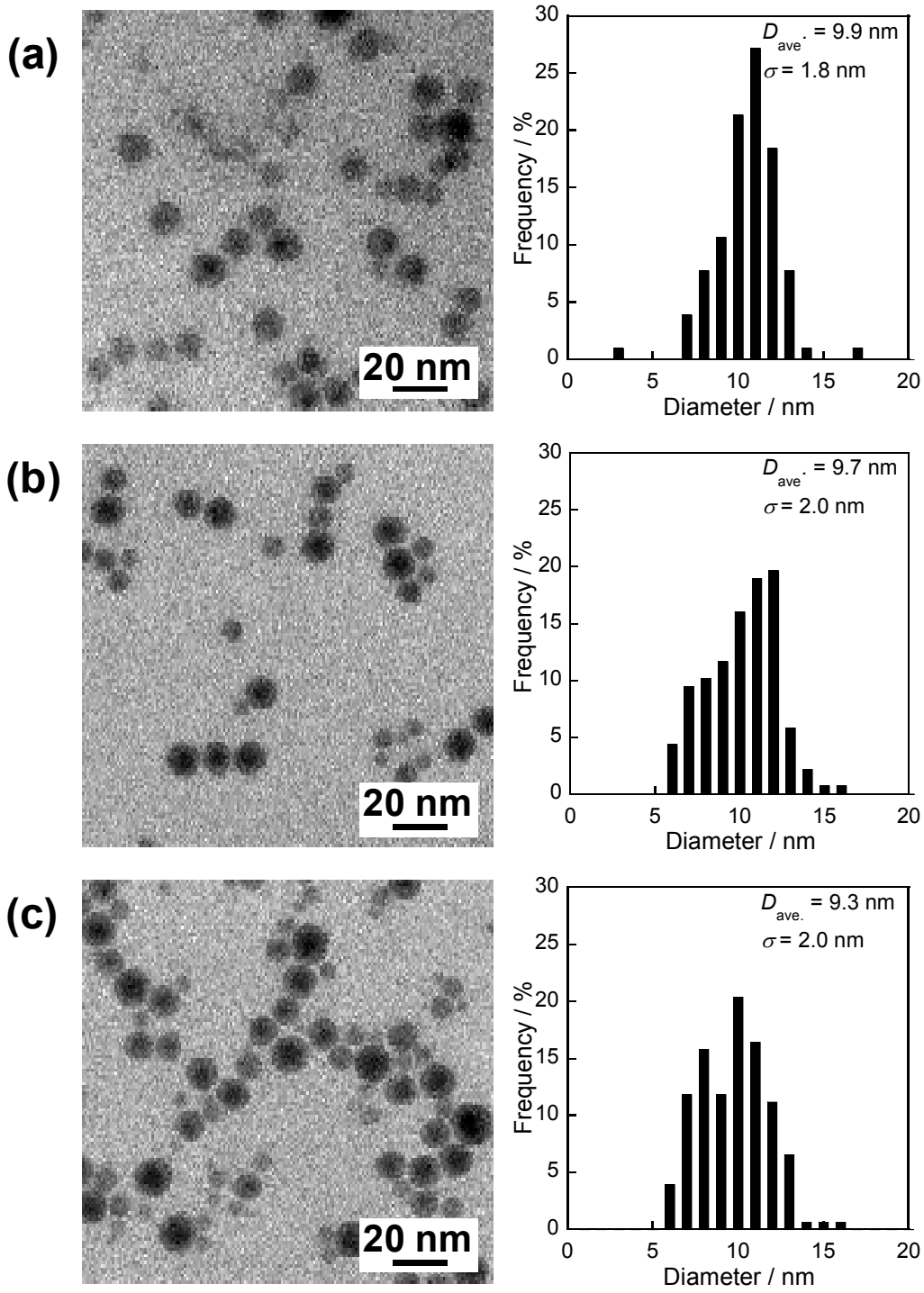

Figure 4.11 TEM images of In nanoparticles sputter deposited in EMI-BF_4 with discharge currents of (a) 5, (b) 10, and (c) 15 mA and their respective histograms.

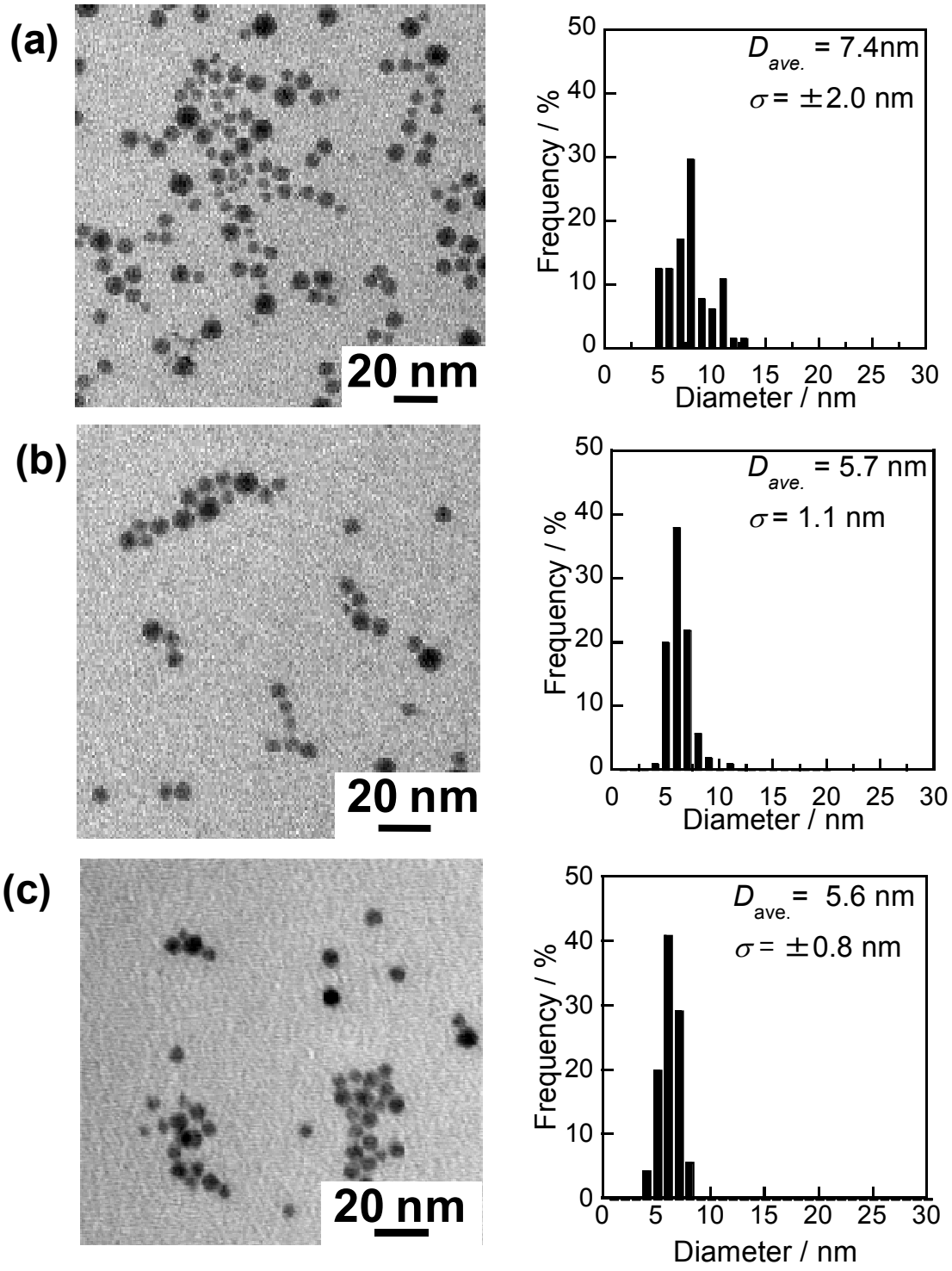

Figure 4.12 Typical TEM images of In/In_2O_3 core/shell nanoparticles prepared by In sputter deposition in HMI-BF_4 (a), OMI-BF_4 (b), and BMMI-BF_4 (c). The size distributions of the particles are also shown beside the corresponding images.

On the contrary, in the case of BMI-TFSA, In nanoparticles could not be confirmed by TEM (Figure 4.14). However, XRF measurement showed existence of In in ILs after sputter deposition of In. The result suggested that the obtained species in the case of TFSA-base ILs may be a cluster of an atom-like species which is too small to observe by our 100 kV TEM instruments.

Hollow nanoparticles made by using three kinds of ILs, BMI-BF_4, AEI-BF_4, and AMI-BF_4. Heat treatment of thus-obtained ILs at 523 K in air changed the nanostructure of nanoparticles as shown in TEM images in Figure 4.15. Although it was difficult to be obtained clear TEM images in the case of using AMI-BF_4, it could be recognized that hollow In_2O_3 nanoparticles were produced in all kinds of ILs used, the size of which was increased with an increase in the whole size of In/In_2O_3 nanoparticles as-sputter-deposited. treatment in ILs. The size of the In metal core seems to linearly increase from 8 to 20 nm by enlargement of the whole size of In/In_2O_3 core/shell nanoparticles. Figure 4.16b shows the In_2O_3 shell thickness of core/shell nanoparticles estimated from the results in Figure 4.16a. Interestingly, the shell thickness was almost constant regardless of the size of core/shell nanoparticles prepared in various kinds of IL. The figure also shows the dependence of d_{void} of the void space on $d_{particle}$ of the hollow In_2O_3 nanoparticles obtained through the shell layer to the In metal core surface from air and/or IL solution at room temperature. Heat treatment of

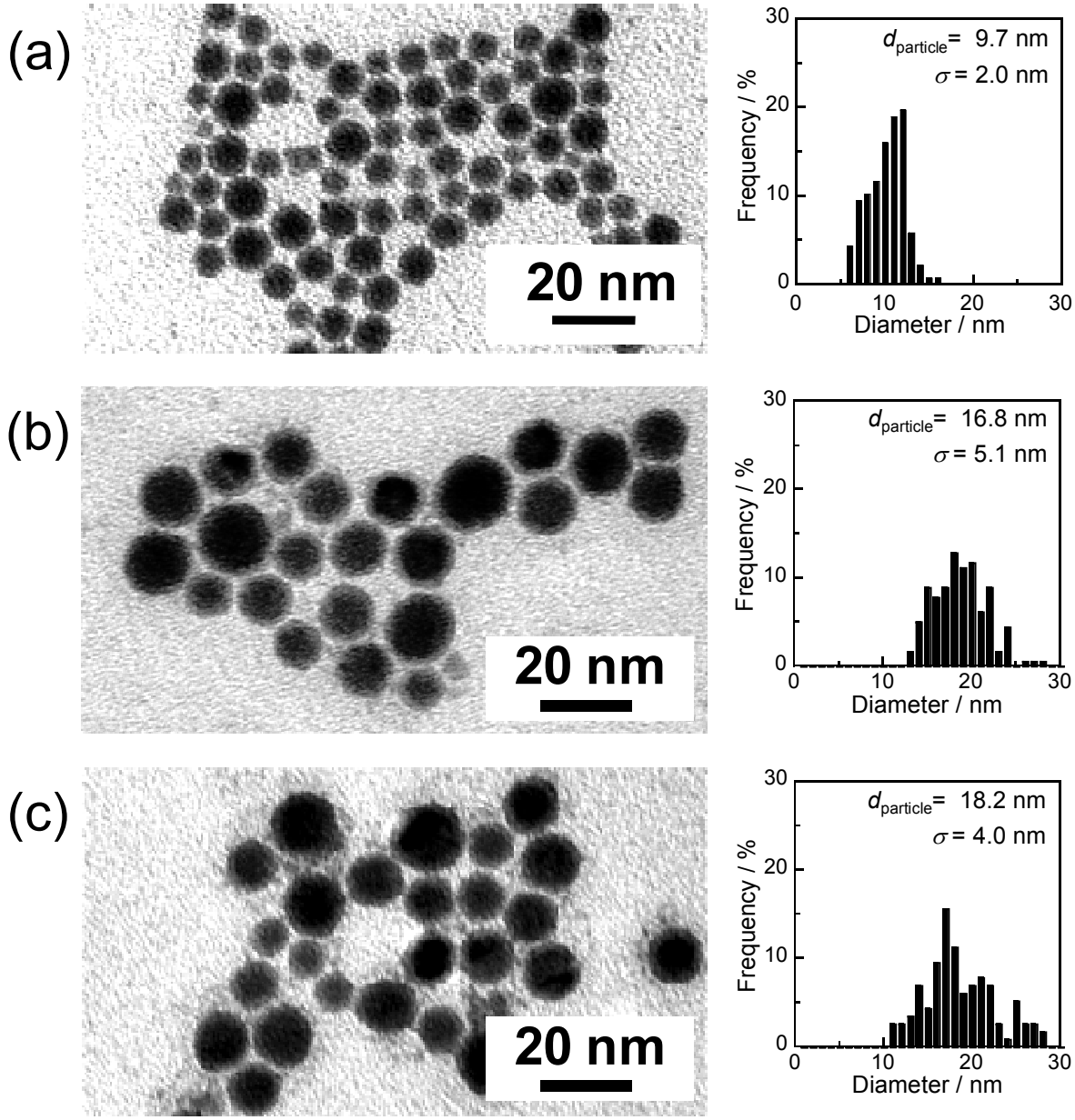

Figure 4.13 Typical TEM images of In/In_2O_3 core/shell nanoparticles prepared by In sputter deposition in BMI-BF_4 (a), AEI-BF_4 (b), and AMI-BF_4 (c). The size distributions of the particles are also shown beside the corresponding images.

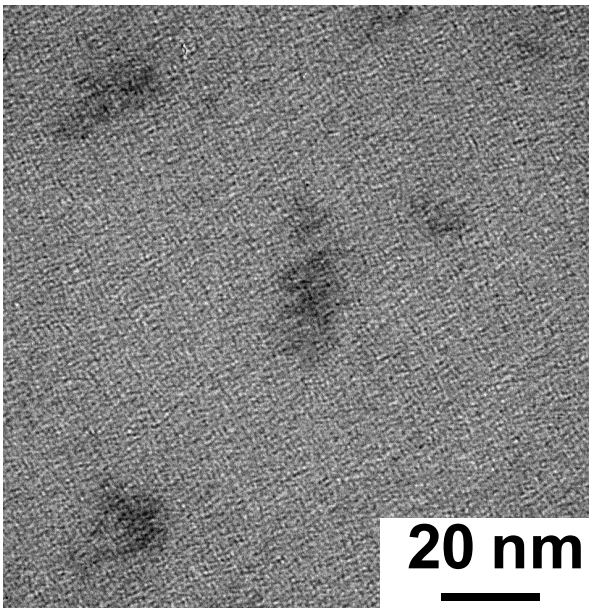

Figure 4.14 Typical TEM images of In nanoparticles prepared by In sputter deposition in BMI-TFSA.

In/In_2O_3 nanoparticles at 523 K.

Figure 4.16a shows average dimensions of the prepared nanoparticles: d_{core} of the In core obtained from TEM measurements is plotted as a function of $d_{particle}$ of In/In_2O_3 after heat produced hollow nanoparticles with a slight increase in $d_{particle}$ (0.1-0.6 nm), except for the case of using AEI-BF_4 as an IL. The value of d_{void} linearly increased from 4 to 10 nm with an increase in $d_{particle}$ of the In core, the average thickness being ca.1.9 nm. This fact indicated that an In_2O_3 shell with a thickness of ca.1.9 nm could effectively prevent the penetration of O_2 hollow nanoparticles, indicating that the structure of thus-obtained hollow In_2O_3 nanoparticles could also be controlled by selecting the kind of IL used for the sputter deposition of In. It should be noted that d_{void} was smaller than d_{core} of the corresponding

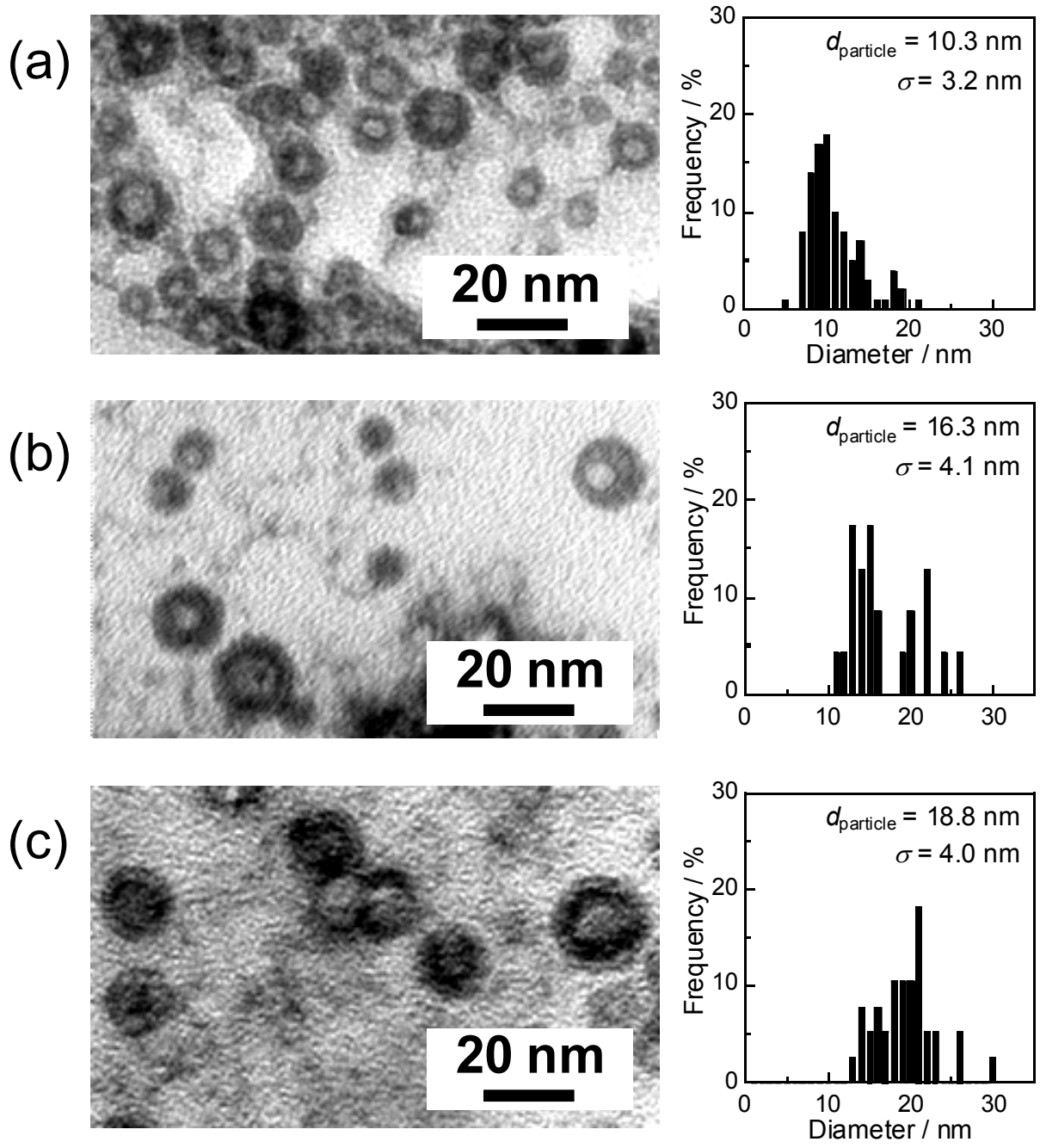

Figure 4.15 Typical TEM images of hollow In_2O_3 nanoparticles prepared by the heat treatment at 523 K. ILs used were BMI-BF_4 (a), AEI-BF_4 (b), and AMI-BF_4 (c). The size distributions of the particles are also shown beside the corresponding images.

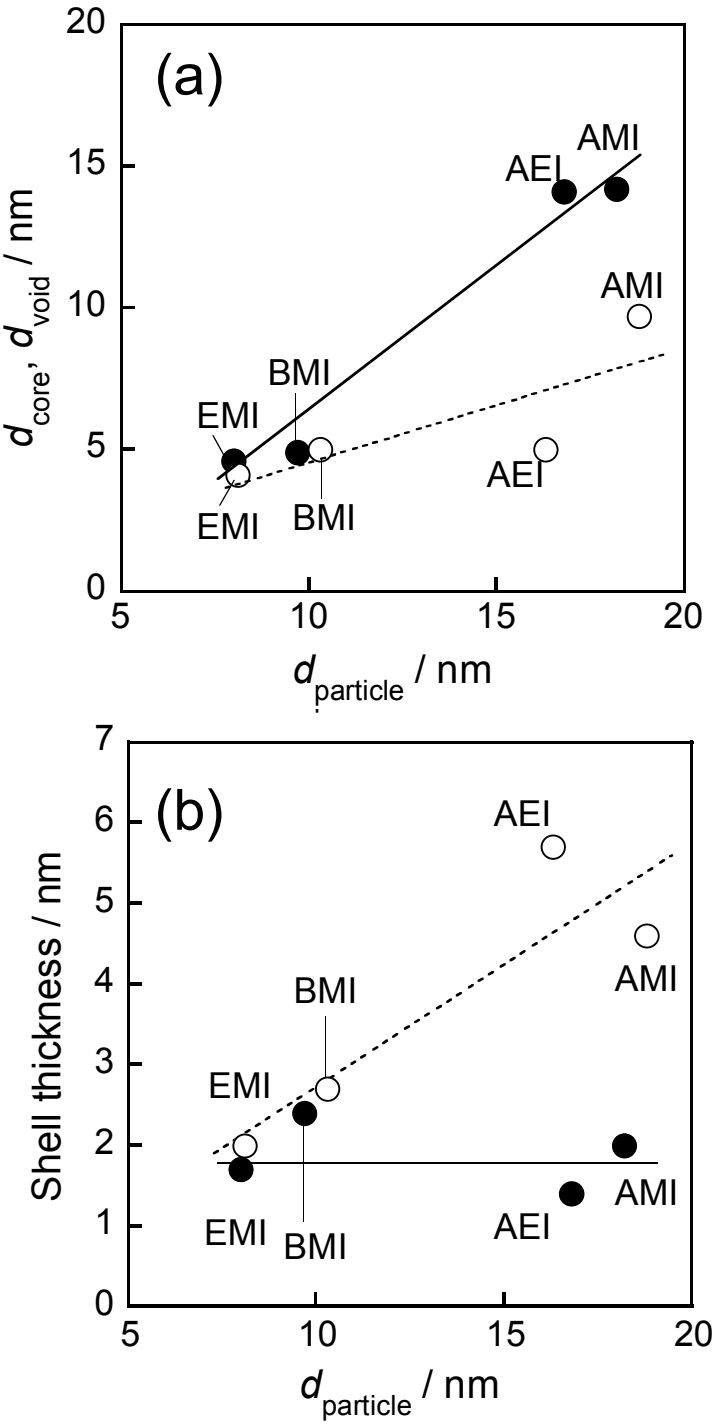

Figure 4.16 (a) Dependence of d_{core} (solid circles) and d_{void} (open circles) on the whole size ($d_{particle}$) of In/In_2O_3 core/shell particles and that of hollow In_2O_3 particles, respectively. (b) Relationship between shell thickness and $d_{particle}$ of In/In_2O_3 core/shell particles (solid circles) or hollow In_2O_3 particles (open circles). Cationic species of ILs used are indicated in the figure.

core/shell nanoparticles (Figure 4.16a). Furthermore, as shown in Figure 4.16b, the shell thickness of hollow nanoparticles was larger than that of In/In_2O_3 nanoparticles (ca.1.9 nm on average) and increased with an increase in $d_{particle}$ of hollow nanoparticles.

The formation of a void space by oxidation of the In metal core with O_2 is reasonably explained by the Kirkendall effect in a nanometer scale.[53,54] Though the In/In_2O_3 core/shell nanoparticles were stable at room temperature because of coverage of the In core with an oxide shell layer to prevent further oxidation of In metal, heat treatment of core/shell nanoparticles in ILs at 523 K, which is higher than the melting point of bulk In metal (419 K), accelerated the oxidation of the In metal core. If only indium ions diffused outward through the shell to form the In_2O_3 oxide layer at the outer surface of the shell, the void space would be formed inside the nanoparticles, the size being comparable to the size of the In core. As shown in Figure 4.16a, the size of the final void space became smaller than that of the initial In metal core, especially for larger In/In_2O_3 nanoparticles. This fact indicated that in addition to the predominant outward diffusion of In ions, an inward transport of oxygen ions occurred, and an In_2O_3 crystal could thus be grown on both the inner concave and outer convex surfaces of the oxide shell layer.

4.4 Conclusion

Sputter deposition of indium in ILs resulted in the production of stable In metal nanoparticles without additional agents, being different from conventional chemical methods using highly active agents to reduce indium ions. The thus-obtained In metal nanoparticles were covered by an amorphous In_2O_3 layer (ca.1.9 nm in thickness), that is, In/In_2O_3 core/shell nanoparticles, the core size of which was tunable from ca.8 to 20 nm depending on the kind of IL used. Heat treatment of thus-obtained nanoparticles at 523 K in air removed the In metal core, resulting in the formation of hollow nanoparticles made of crystalline In_2O_3, the void space of which could be enlarged from 4 to 10 nm by increasing the size of core/shell nanoparticles used as the starting material. The sizes of both In/In_2O_3 core/shell nanoparticles and hollow In_2O_3 nanoparticles were controlled by selecting an appropriate kind of IL. Since In metal nanoparticles are useful as a starting material to convert them to In-based compound materials, such as InP quantum dots,[55] the size tunability of In nanoparticles obtained by the present strategy will enable precise control of the nanostructure of the resulting target materials. On the other hand, In_2O_3 is well known as an n-type semiconducting oxide having a band gap of around 3.6 eV. Precise control of the hollow structure of In_2O_3 nanoparticles should lead to the development of novel photocatalysts for

molecular-size-selective reactions and for solar cells, in which the void space can act as a nano-flask for reaction sites and/or molecular adsorption sites.

4.5 References

(1) Kamat, P. *J. Phys. Chem. C* **2007**, *111*, 2834.

(2) Muszynski, R.; Seger, B.; Kamat, P. *J. Phys Chem. C* **2008**, *112*, 5263.

(3) Caruso, F.; Spasova, M.; Saigueirino-Maceira, V.; Liz-Marzan, L. *Adv. Mater.* **2001**, *13*, 1090.

(4) Riha, S.; Parkinson, B.; Prieto, A. *J. Am. Chem. Soc.* **2009**, *131*, 12054.

(5) Nakashima, T.; Kobayashi, Y.; Kawai, T. *J. Am. Chem. Soc.* **2009**, *131*, 11302.

(6) Saruyama, M.; Kanehara, M.; Teranishi, T. *J. Am. Chem. Soc.* **2010**, *132*, 3280.

(7) Scheeren, C.; Machado, G.; Dupont, J.; Fichtner, P.; Texeira, S. *Inorg. Chem.* **2003**, *42*, 4738.

(8) Migowski, P.; Machado, G.; Texeira, S.; Alves, M.; Morais, J.; Traverse, A.; Dupont, J. *Phys. Chem. Chem. Phys.* **2007**, *9*, 4814.

(9) Redel, E.; Thomann, R.; Janiak, C. *Chem. Commun.* **2008**, 1789.

(10) Dupont, J.; Fonseca, G.; Umpierre, A.; Fichtner, P.; Teixeira, S. *J. Am. Chem. Soc.* **2002**, *124*, 4228.

(11) Fonseca, G.; Umpierre, A.; Fichtner, P.; Teixeira, S.; Dupont, J. *Chem. Eur. J.* **2003**, *9*, 3263.

(12) Guo, S.; Shi, F.; Gu, Y.; Yang, J.; Deng, Y. *Chem. Lett.* **2005**, *34*, 830.

(13) Kuwabata, S.; Kongkanand, A.; Oyamatsu, D.; Torimoto, T. *Chem. Lett.* **2006**, *35*, 600.

(14) Smith, E.; Villar Garcia, I.; Briggs, D.; Licence, P. *Chem. Commun.* **2005**, 5633.

(15) El Abedin, S.; Polleth, M.; Meiss, S.; Janek, J.; Endres, F. *Green Chem.* **2007**, *9*, 549.

(16) Meiss, S.; Rohnke, M.; Kienle, L.; El Abedin, S.; Endres, F.; Janek, J. *ChemPhysChem* **2007**, *8*, 50.

(17) Torimoto, T.; Okazaki, K.; Kiyama, T.; Hirahara, K.; Tanaka, N.; Kuwabata, S. *Appl. Phys. Lett.* **2006**, *89*, 243117.

(18) Okazaki, K.; Kiyama, T.; Hirahara, K.; Tanaka, N.; Kuwabata, S.; Torimoto, T. *Chem. Commun.* **2008**, 691.

(19) Suzuki, T.; Okazaki, K.; Kiyama, T.; Kuwabata, S.; Torimoto, T. *Electrochemistry* **2009**, *77*, 638.

(20) Tsuda, T.; Kurihara, T.; Hoshino, Y.; Kiyama, T.; Okazaki, K.; Torimoto, T.; Kuwabata, S. *Electrochemistry* **2009**, *77*, 693.

(21) Okazaki, K.; Kiyama, T.; Suzuki, T.; Kuwabata, S.; Torimoto, T., *Chem. Lett.* **2009**, 38, 330.

(22) Kameyama, T.; Ohno, Y.; Kurimoto, T.; Okazaki, K.; Uematsu, T.; Kuwabata, S.; Torimoto, T., *Phys. Chem. Chem. Phy.* **2010**, 12, 1804.

(23) Khatri, O. P.; Adachi, K.; Murase, K.; Okazaki, K.; Torimoto, T.; Tanaka, N.; Kuwabata, S.; Sugimura, H., *Langmuir* **2008**, 24, 7785.

(24) Tsuda, T.; Yoshii, K.; Torimoto, T.; Kuwabata, S., *J. Power Sources* **2010**, 195, 5980.

(25) Torimoto, T.; Tsuda, T.; Okazaki, K.; Kuwabata, S., *Adv. Mater*. **2010**, 22, 1196.

(26) Kuwabata, S.; Tsuda, T.; Torimoto, T., *J. Phys. Chem. Lett.* **2010**, 1, 3177.

(27) Suzuki, T.; Suzuki, S.; Okazaki, K.; Shibayama, T.; Kuwabata, S.; Torimoto, T. *Chem. Lett.* **2010**, 39, 1072.

(28) Oda, Y.; Hirano, K.; Yoshii, K.; Kuwabata, S.; Torimoto, T.; Miura M. *Chem. Lett.* **2010**, 39, 1069.

(29) Li, C.; Zhang, D.; Han, S.; Liu, X.; Tang, T.; Zhou, C. *Adv. Mater.* **2003**, *15*, 143.

(30) Dimitrijevic, N.; Rajh, T.; Ahrenkiel, S.; Nedeljkovic, J.; Micic, O.; Nozik, A. *J. Phys. Chem. B* **2005**, *109*, 18243.

(31) Dayeh, S.; Yu, E.; Wang, D. *small* **2007**, *3*, 1683.

(32) Hammarberg, E.; Feldmann, C. *Chem. Mater.* **2009**, *21*, 771.

(33) Soulantica, K.; Maisonnat, A.; Fromen, M.; Casanove, M.; Lecante, P.; Chaudret, B. *Angew. Chem. Int. Ed.* **2001**, *40*, 448.

(34) Ganeev, R.; Ryasnyanskiy, A.; Chakravarty, U.; Naik, P.; Srivastava, H.; Tiwari, M.; Gupta, P., S *Appl. Phys. B* **2007**, *86*, 337.

(35) Chen, Q.; Tanaka, M.; Furuya, K. *Surf. Sci*. **1999**, *440*, 398.

(36) Zhao, Y.; Zhang, Z.; Dang, H. *J. Phys. Chem. B* **2003**, *107*, 7574.

(37) Du, N.; Zhang, H.; Chen, B.; Ma, X.; Liu, Z.; Wu, J.; Yang, D. *Adv. Mater.* **2007**, 19, 1641.

(38) van de Lagemaat, J.; Barnes, T.; Rumbles, G.; Shaheen, S.; Coutts, T.; Weeks, C.; Levitsky, I.; Peltola, J.; Glatkowski, P. *Appl. Phys. Lett.* **2006**, *88*, 233503.

(39) Minami, T.; Takata, S.; Kakumu, T. *J. Vac. Sci. Technol. A* **1996**, *14*, 1689.

(40) Li, B.; Xie, Y.; Jing, M.; Rong, G.; Tang, Y.; Zhang, G. *Langmuir* **2006**, *22*, 9380.

(41) Joint Committee on Powder Diffraction Standards (JCPDS), International Center for Diffraction Data, Swarthmore, PA 1992, File 5-642.

(42) Joint Committee on Powder Diffraction Standards (JCPDS), International Center for Diffraction Data, Swarthmore, PA 1992, File 6-416.

(43) Nair, P.; Radhakrishnan, T.; Revaprasadu, N.; Kolawole, G.; O'Brien, P. *J. Mater. Chem.* **2002**, *12*, 2722.

(44) Lei, Y.; Chim, W., *J. Am. Chem. Soc.* **2005**, *127*, 1487.

(45) Balamurugan, B.; Kruis, F.; Shivaprasad, S.; Dmitrieva, O.; Zahres, H. *Appl. Phys. Lett*. **2005**, *86*, 083102.

(46) Faur, M.; Faur, M.; Jayne, D. T.; Goradia, M.; Goradia, C. *Surf. Interface Anal.* **1990**, *15*, 641.

(47) Nefedov, V. I.; Gati, D.; Dzhurinskii, B. F.; Sergushin, N. P.; Salyn, Y. V. *Zh. Neorg. Khim*. **1975**, *20*, 2307.

(48) Khanna, P.; Jun, K.; Hong, K.; Baeg, J.; Chikate, R.; Das, B. *Mater. Lett.* **2005**, *59*, 1032.

(49) Zayed, M.; Hegazy, M.; Elsayed-Ali, H. *Thin Solid Films* **2004**, *449*, 254.

(50) Hatakeyama, Y.; Okamoto, M.; Torimoto, T.; Kuwabata, S.; Nishikawa, K.,. *J. Phys. Chem.C* **2009**, 113, 3917.

(51) Hatakeyama, Y.; Takahashi, S.; Nishikawa, K., *J. Phys. Chem.C* **2010**, 114, 11098.

(52) Wender, H.; de Oliveira, L. F.; Migowski, P.; Feil, A. F.; Lissner, E.; Prechtl, M. H. G.; Teixeira, S. R.; Dupont, J., *J. Phys. Chem.C* **2010**, 114, 11764.

(53) Yin, Y.; Rioux, R.; Erdonmez, C.; Hughes, S.; Somorjai, G.; Alivisatos, A. *Science* **2004**, *304*, 711.

(54) Fan, H.; Gosele, U.; Zacharias, M. *small* **2007**, *3*, 1660.

(55) Nedeljkovic, J.; Micic, O.; Ahrenkiel, S.; Miedaner, A.; Nozik, A. *J. Am. Chem. Soc*. **2004**, *126*, 2632.

Chapter 5 General Conclusion

5.1 Summary and prospect

The present thesis is concerned with synthesis of nanoparticles using a chemical reaction induced by sputter deposition of metal onto ionic liquids (ILs). The remarked results are as follows: In Chapter 2, the sputter deposition of silver (Ag) onto IL produced Ag nanoparticles whose size was varied greatly dependent on the sputtering conditions. Change in the discharge current from 10 to 40 mA increased Ag particle size from 5.7 to 11 nm, though prolongation of sputtering time simply caused a higher concentration of Ag nanoparticles in IL without change in their size. Sputter deposition of Ag onto IL solutions containing $HAuCl_4$ resulted in the appearance of a single surface plasmon resonance peak in the absorption spectra of the resulting solution, and their peak position was red-shifted with an increase in the concentration of $HAuCl_4$. The obtained results clearly indicated that Ag metal species sputter-deposited in IL can reduce $HAuCl_4$ to give AuAg alloy nanoparticles and that their chemical composition varies depending on the initial concentration of $HAuCl_4$.

In Chapter 3, the sputter deposition of transition metals tungsten (W), molybdenum (Mo), niobium (Nb), and titanium (Ti) onto IL produced corresponding metal oxide

nanoparticles smaller than 6 nm. The obtained naoparticles were composites composed of metal and oxide and a highly dispersed manner without in IL any additional stabilizing agents in IL.

In Chapter 4, the sputter deposition of indium (In) in ILs could produce stable In metal nanoparticles whose surface was covered by an amorphous In_2O_3 layer to form In/In_2O_3 core/shell nanoparticles. The size of the In core was tunable from ca. 8 to 20 nm by selecting the kind of IL, where as the shell thickness of In_2O_3 was almost constant at ca. 1.9 nm. Heat treatment of the thus-obtained nanoparticles at 523K in air oxidized In metal of the core, resulting in the formation of spherical hollow nanoparticles made of crystalline In_2O_3. The size of the hollow nanoparticles was slightly larger than that of the In/In_2O_3 core/shell nanoparticles used as starting materials, where as the void space formed inside hollow nanoparticles was smaller than the corresponding In metal cores. These facts indicated that in addition to the predominant outward diffusion of In ions, an inward transport of oxygen ions occurred, and thus an In_2O_3 crystal could be grown on both the inner concave and outer convex surfaces of the oxide shell layer.

Desired metal nanoparticles can be prepared by the sputter deposition of the corresponding metal onto ILs. I demonstrated in this thesis that the chemical reactions induced by the sputter-deposited metal species were useful to modify the nanostructure of the

resulting nanoparticles. Especially, nanoparticles of highly reactive In metals, which was difficult to be synthesized by the conventional solution methods, could be easily prepared by this sputtering technique and worked as a precursor to prepare hollow In_2O_3 nanoparticles by the oxidation of In metal, void space of which was tunable depending on the size of precursor nanoparticles. Though the spherical nanoparticles were reported in the present study, the combination of the sputter deposition technique with the chemical reaction in ILs will enable the designing of nanostructured particles having anisotropic shapes with various kinds of materials, which are suitable for various applications, such as drug delivery systems, catalytic reactions, sensors, and solar light energy conversion systems. I expect that the findings in the present thesis will open a way to develop novel functional materials using colloidal nanostructured particles in near future.

List of Publications

Papers

1. A Facile Synthesis of AuAg Alloy Nanoparticles Using a Chemical Reaction Induced by Sputter Deposition of Metal onto Ionic Liquids

   Toshimasa Suzuki, Ken-ichi Okazaki, Tomonori Kiyama, Susumu Kuwabata, and Tsukasa Torimoto

   Electrochemistry 77, 636 (2009)

2. Fabrication of Transition Metal Oxide Nanoparticles Highly Dispersed in Ionic Liquids by a Sputter Deposition Technique Authors

   Toshimasa Suzuki, Shushi Suzuki, Yousuke Tomita, Ken-ichi Okazaki, Tamaki Shibayama, Susumu Kuwabata, and Tsukasa Torimoto

   Chem. Lett. 39, 1072 (2010)

3. Nanosize-controlled Syntheses of Indium Metal Particles and Hollow Indium Oxide Particles via the Sputter Deposition Technique in Ionic Liquids

   Toshimasa Suzuki, Ken-ichi Okazaki, Shushi Suzuki, Tamaki Shibayama, Susumu Kuwabata, Tsukasa Torimoto

   Chem. Mater. 22, 5209 (2010)

The papers not included in the present thesis:

1. Thermally Induced Self-assembly of Gold Nanoparticles Sputter-deposited in Ionic Liquids on Highly Ordered Pyrolytic Graphite Surfaces

   Ken-ichi Okazaki, Tomonori Kiyama, Toshimasa Suzuki, Susumu Kuwabata, and Tsukasa Torimoto

   Chem. Lett. 38, 330 (2009)

Conferences

1. "Preparation of AuAg Alloy Nanoparticles by the Reduction of $AuCl_4$- ions with Ag Nanoparticles Sputter-Deposited in Ionic Liquids"

   ○Toshimasa Suzuki, Tomonori Kiyama, Ken-ichi Okazaki, Susumu Kuwabata, and Tsukasa Torimoto

   Nagoya University Joint Symposia: 5th Yoshimasa Hirata Memorial Lecture and The 1st Global COE International Symposium on Elucidation and Design of Materials and Molecular Functions 13-14 January 2009, Nagoya, Japan.

2. "Preparation of AuAg Alloy Nanoparticles Using a Chemical Reaction Induced by Sputter Deposition of Metal onto Ionic Liquids"

   ○Toshimasa Suzuki, Ken-ichi Okazaki, Tomonori Kiyama, Susumu Kuwabata, and T. Tsukasa Torimoto

   3rd Congress on Ionic Liquids May 31 - June 4 2009, Cairns Convention Centre, Cairns Australia.

3. “Synthesis of AuAg Alloy Nanoparticles Using a Chemical Reaction Induced by Ag Particles Sputter-deposited in Ionic Liquids”

   ○Toshimasa Suzuki, Ken-ichi Okazaki, Tomonori Kiyama, Susumu Kuwabata, and Tsukasa Torimoto

   2009 Tsinghua Univ.-Nagoya Univ. -Toyota Motor Corp. Joint Symposium on Advanced Materials December 10, 2009, Haikou, China.

4. “Synthesis of Indium Nanoparticles and Hollow Indium Oxide Nanoparticles by the Sputter Deposition in Ionic Liquids”

   ○Toshimasa Suzuki, Ken-ichi Okazaki, Shushi Suzuki, Tamaki Shibayama, Susumu Kuwabata, and Tsukasa Torimoto.

   International Conference on Nanoscopic Colloid and Surface Science September 19-22, 2010, Chiba, Japan.

5. “Syntheses of Indium Metal Particles and Hollow Indium Oxide Particles by the Sputter Deposition Technique in Ionic Liquids”

   ○Toshimasa Suzuki, Ken-ichi Okazaki, Shushi Suzuki, Tamaki Shibayama, Susumu Kuwabata, and Tsukasa Torimoto.

   218th ECS Meeting October 10-15, 2010, Las Vegas, USA.

6. “イオン液体中における金属粒子の化学反応を利用した新規ナノ構造体の作製”

   ○鈴木 俊正, 木山 朋紀, 岡崎 健一, 桑畑 進, 鳥本 司, ,

   第 39 回中部化学関係学協会支部連合秋季大会, 8-9 Noember 2008, 名古屋大学, 愛知.

7. “イオン液体への金属のスパッタ蒸着による AuAg 合金ナノ粒子の作製”

○鈴木 俊正, 岡崎 健一, 桑畑 進, 鳥本 司

第 2 回 物質科学フロンティアセミナー ,12-13 March 2009, 名古屋大学, 名古屋.

8. “溶液内化学反応を伴うイオン液体への金属スパッタ蒸着による合金ナノ粒子の作製”,

○鈴木 俊正, 岡崎 健一, 桑畑 進, 鳥本 司

電気化学会第 76 回大会, 29-31 March 2009, 京都大学, 京都.

9. “イオン液体中での金属ナノ粒子の化学反応を利用する新規ナノ構造体の作製”,

○鈴木 俊正, 岡崎 健一, 桑畑 進, 鳥本 司

第 62 回コロイドおよび界面化学討論会, 17-19 September 2009, 岡山理科大学, 岡山.

10. “イオン液体への金属スパッタ蒸着法を用いる中空酸化インジウムナノ粒子の作製”

○鈴木 俊正, 岡崎 健一, 鈴木 秀士, 柴山 環樹, 桑畑 進, 鳥本 司

電気化学会第 77 回大会, 29-31 March 2010, 富山大学, 富山.

11. “イオン液体へのスパッタ蒸着法を用いる酸化インジウム中空ナノ粒子の作製”

○鈴木 俊正, 岡崎 健一, 鈴木 秀士, 柴山 環樹, 桑畑 進, 鳥本 司

応用物理学会第 71 回秋季講演会, 14-17 September 2010, 長崎大学, 長崎.

12. “イオン液体へのスパッタ蒸着法を用いるコアシェル構造インジウムナノ粒子の

作製”

○鈴木 俊正, 岡崎 健一, 鈴木 秀士, 柴山 環樹, 桑畑 進, 鳥本 司

第 4 回 物質科学フロンティアセミナー, 19-20 November 2010, 名古屋大学, 名古屋.

Patent

1. 鳥本 司, 鈴木 俊正, 岡崎 健一, 冨田 庸介, 桑畑 進

「中空ナノ粒子の製法」,

特願 2009-258325

Award

1. “Synthesis of Indium Nanoparticles and Hollow Indium Oxide Nanoparticles by the Sputter Deposition in Ionic Liquids”

Best Poster Award in International Conference on Nanoscopic Colloid and Surface Science, 19-22 September 2010, Chiba, Japan.

Acknowledgement

The author would like to express his science gratitude to Professor Tsukasa Torimoto for their continuous guidance and encouragement throughout the work of this thesis.

The author would like to thank Associate Professor Shushi Suzuki and Assistant Professor Ken-ichi Okazaki for their helpful and useful comments and suggestions.

The author is very grateful acknowledge to Professor Susumu Kuwabata and Assistant Professor Tetsuya Tsuda (Department of Applied Chemistry, Graduate School of Engineering, Osaka University) for their helpful and useful comments and suggestions.

The author makes grateful acknowledgement to Associate Professor Tamaki Shibayama, (Center for Advanced Research of Energy Coversion Materials, Hokkaido University) for their corporations on TEM observation.

The author wishes to thank Assistant Keiko Miyagawa and all members in Laboratory of Molecular Design Chemistry (Torimoto Laboratory).

Finally, the author would like to deeply express his acknowledgement to his family for their continuous supports and encouragements throughout study.

December 2011

Toshimasa Suzuki